AGU PUBLICATIONS

JGR

Journal of Geophysical Research: Oceans

RESEARCH ARTICLE

10.1002/2013JC009004

Companion to *Yao et al.* [2014] doi:10.1002/2013JC009331.

**Key Points:**

- Overturning circulation in the Red Sea is successfully simulated with MITgcm
- During summer, the GAIW enters the Red Sea as an eastern boundary current
- Remote and local winds and latitudinally differential heating control intrusion

**Correspondence to:**
I. Hoteit,
ibrahim.hoteit@kaust.edu.sa

**Citation:**
Yao, F., I. Hoteit, L. J. Pratt, A. S. Bower, P. Zhai, A. Köhl, and G. Gopalakrishnan (2014), Seasonal overturning circulation in the Red Sea: 1. Model validation and summer circulation, *J. Geophys. Res. Oceans*, *119*, 2238–2262, doi:10.1002/2013JC009004.

Received 9 APR 2013
Accepted 10 MAR 2014
Accepted article online 17 MAR 2014
Published online 14 APR 2014

# Seasonal overturning circulation in the Red Sea: 1. Model validation and summer circulation

**Fengchao Yao[1], Ibrahim Hoteit[1], Larry J. Pratt[2], Amy S. Bower[2], Ping Zhai[2], Armin Köhl[3], and Ganesh Gopalakrishnan[4]**

[1]Division of Physical Sciences and Engineering, King Abdullah University of Science and Technology, Thuwal, Saudi Arabia, [2]Department of Physical Oceanography, Woods Hole Oceanographic Institution, Woods Hole, Massachusetts, USA, [3]Institut für Meereskunde, Zentrum für Meeres- und Klimaforschung, Universität Hamburg, Hamburg, Germany, [4]Scripps Institution of Oceanography, Nierenberg Hall, San Diego, California, USA

**Abstract** The overturning circulation in the Red Sea exhibits a distinct seasonally reversing pattern and is studied using high-resolution MIT general circulation model simulations. In the first part of this study, the vertical and horizontal structure of the summer overturning circulation and its dynamical mechanisms are presented from the model results. The seasonal water exchange in the Strait of Bab el Mandeb is successfully simulated, and the structures of the intruding subsurface Gulf of Aden intermediate water are in good agreement with summer observations in 2011. The model results suggest that the summer overturning circulation is driven by the combined effect of the shoaling of the thermocline in the Gulf of Aden resulting from remote winds in the Arabian Sea and an upward surface slope from the Red Sea to the Gulf of Aden set up by local surface winds in the Red Sea. In addition, during late summer two processes associated, respectively, with latitudinally differential heating and increased salinity in the southern Red Sea act together to cause the reversal of the contrast of the vertical density structure and the cessation of the summer overturning circulation. Dynamically, the subsurface northward pressure gradient force is mainly balanced by vertical viscosity resulting from the vertical shear and boundary friction in the Strait of Bab el Mandeb. Unlike some previous studies, the three-layer summer exchange flows in the Strait of Bab el Mandeb do not appear to be hydraulically controlled.

## 1. Introduction

The Red Sea is a narrow and long semienclosed basin, lying between the Asian and African continents and extending from 12.5°N to 30°N in the NW-SE direction. The average depth in the Red Sea is approximately 490 m, but an axial trench with depths >2000 m exists. The Red Sea is connected to the Gulf of Aden and the Indian Ocean by the Strait of Bab el Mandeb (referred to as the strait hereinafter), which is an approximately 150 km long channel (Figure 1). The shallowest sill, the Hanish Sill, is located at the northern end of the strait, and the narrowest contraction is located at the Perim Narrows in the southern end of the strait [*Murray and Johns*, 1997; *Sofianos et al.*, 2002]. In the northern end two small gulfs, the Gulf of Suez and the Gulf of Aqaba are connected to the Red Sea. The Gulf of Suez is a shallow basin with maximum depths <100 m. In contrast, the Gulf of Aqaba is a miniature of the Red Sea with maximum depths >1800 m and is connected to the Red Sea through a 260 m deep sill in the Strait of Tiran.

The Red Sea is a concentration basin where one of the most saline water masses (>40 psu) is produced due to excess of evaporation over precipitation and limited water exchange with the open ocean through the strait. This saline water is exported through the strait as a deep outflow, reaches its neutral buoyancy level around 800 m after intensive mixing with ambient fresher water in the Gulf of Aden, and spreads laterally as a subsurface salinity maximum in the Indian Ocean [*Bower et al.*, 2000; *Beal et al.*, 2000].

There have been no direct current observations of the overturning circulations associated with the formation and export of the saline water mass in the Red Sea. While the temperature and salinity are almost uniform below the pycnocline (200–300 m) in the Red Sea, distributions of geochemical tracers, such as $^{14}C$ and $^{3}He$, and dissolved oxygen concentration suggest a two-cell overturning circulation structure in the Red Sea [*Cember*, 1988; *Eshel et al.*, 1994]. On top is an overturning cell composed of a surface mean inflow and

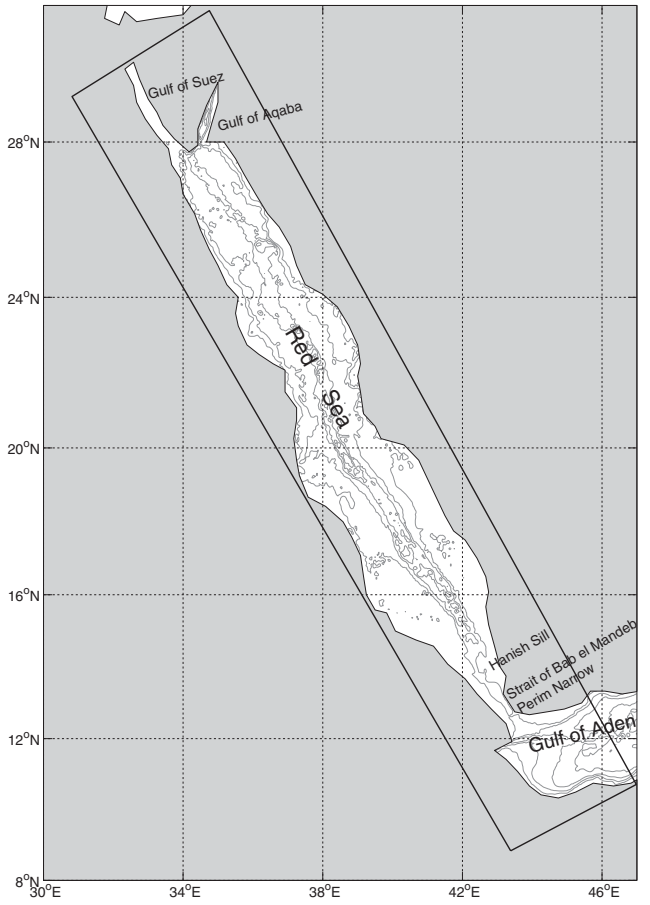


**Figure 1.** Bathymetry of the Red Sea. Contours intervals are 500 m starting from 100 m. The model domain is indicated by the black box. Boundary conditions are specified in the Gulf of Aden along the eastern side of the domain.

a mean outflow immediately below the pycnocline. Additionally, there exists a deep opposing weaker overturning cell consisting of a bottom southward flow and an intermediate returning northward flow at about 500 m [*Cember*, 1988]. The deep cell is thought by *Woelk and Quadfasel* [1996] to be driven by overflows from the Gulf of Suez formed intermittently during anomalously cold winters. However, observations [*Plahn et al*., 2002; *Manasrah et al*., 2004] suggest that the densest water mass in the northern Red Sea is supplied from the Gulf of Aqaba. The boundary between these two overturning cells is readily identified by the contrast of the dissolved oxygen concentration; the water mass formed from the convection in the shallow cell is distinguished from the Red Sea Deep Water (RSDW) by its much higher dissolved oxygen concentration [*Woelk and Quadfasel*, 1996; *Sofianos and Johns*, 2007]. This water is referred to as the Red Sea Intermediate Water (RSIW) here and constitutes most of the deep outflow in the strait [*Sofianos and Johns*, 2003, *Yao et al*., 2014]. As suggested by the observations of *Sofianos and Johns* [2007], the RSDW also possibly contributes to the deep outflow in the strait. The deep outflow consisting of the RSIW and RSDW in the strait is referred to as the Red Sea Outflow Water (RSOW). In this study we focus on the shallow upper overturning cell.

The shallow overturning circulation in the Red Sea is found to have a drastic seasonally reversing pattern [e.g., *Smeed*, 1997]. During winter, a typical vertical distribution of water properties for a convective overturning is established, consisting of a surface layer with gradually increased salinity and decreased temperature northward and a cold and high-salinity deep layer [e.g., *Patzert*, 1974]. In contrast, summer hydrographic observations along the axis of the Red Sea clearly show a subsurface intrusion of the Gulf of Aden Intermediate Water (GAIW) represented by fresher and colder waters [*Maillard and Soliman*, 1986; *Sofianos and Johns*, 2007]. The 18 month long-term observations of the water exchange in the strait during 1995–1996 described by *Sofianos et al*. [2002] confirms that this seasonal overturning pattern is a robust feature. In winter, a typical two-layer exchange structure, with a fresher inflow from the Gulf of Aden on top of an outflow from the Red Sea, is established. In summer months (June to September), this circulation pattern is changed to a three-layer structure: a surface outflow from the Red Sea on top of a subsurface intrusion of the GAIW and a much weaker (even vanishing) deep outflow. In paleoclimate studies, *Biton et al*. [2008, 2010] found in their simulations using the MITgcm that the seasonal transition to a three-layer exchange flow in the strait is a robust feature under very different atmospheric conditions and sea levels during the glacial and interglacial periods.

The Red Sea is subject to seasonally varying atmospheric forcing, which is responsible for driving the seasonal overturning circulation in the basin and water exchange through the strait. The annual mean net fresh

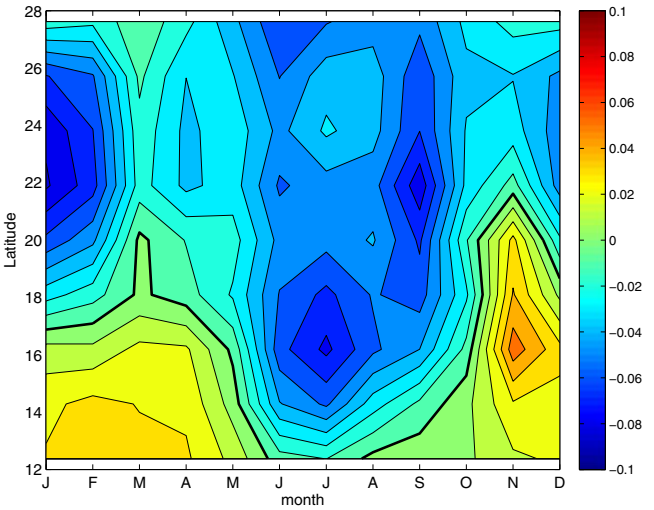


**Figure 2.** Annual cycle of the surface wind stress (Pa) rotated along the axis of the Red Sea averaged from the NCEP reanalysis data in 1980. Positive values indicate wind stress toward northwest. The surface winds in the south Red Sea reverse from southeasterly to northwesterly in summer (June to September).

water loss over the surface is estimated to be 2.06 ± 0.22 m $yr^{-1}$, and the heat flux has a relatively small annual mean heat loss of 11 ± 5 W $m^{-2}$ but a large annual cycle with a range of about 200 W $m^{-2}$ [*Sofianos et al.*, 2002]. Influenced by the Indian monsoon, the summer surface wind field (June to September) in the southern Red Sea reverses from southeasterly to northwesterly, while the winds in the northern Red Sea remain northwesterly throughout the year (Figure 2). Meanwhile, the winds in the Gulf of Aden also change from easterly to westerly in summer.

Because of its elongated shape, the overturning circulation in the Red Sea or a similar idealized basin is often treated two-dimensionally in analytical or modeling studies [*Phillips*, 1966; *Tragou and Garrett*, 1997; *Finnigan et al.*, 2001]. However, three-dimensional modeling studies have shown that the circulation in the Red Sea exhibits complex spatial structures [*Clifford et al.*, 1997; *Eshel and Naik*, 1997; *Sofianos and Johns*, 2002, 2003; *Biton et al.*, 2008, 2010]. In *Sofianos and Johns* [2002, 2003], an isopycnic modeling simulation forced by monthly climatology atmospheric forcing simulated energetic meso-scale eddies and boundary currents both along the western coast and the eastern coast. Even though the basic seasonal overturning structure is captured, the detailed vertical structures of the overturning circulation in the Red Sea are not well established due to the coarse resolution (∼10 km) of the model. The dynamical processes that drive the seasonal overturning circulation remain obscure. Furthermore, recent studies by *Belkin* [2009] and *Raitsos et al.* [2011] suggest that there has been a rapid warming trend in the Red Sea since the last decade, and understanding the warming mechanisms also requires a clearer dynamical picture of the circulation in the Red Sea.

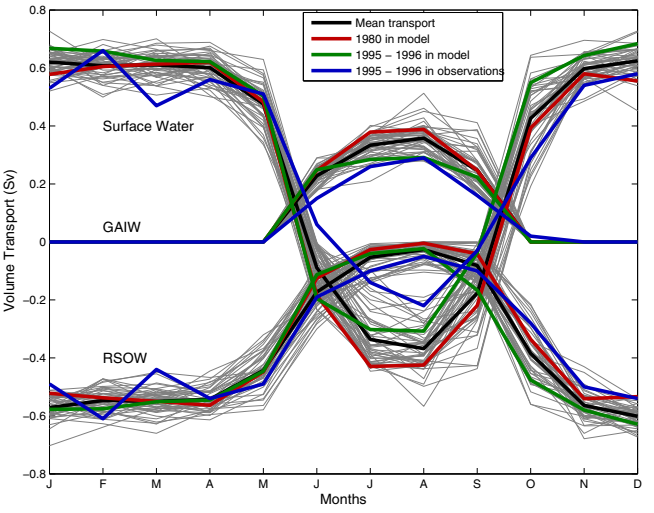


**Figure 3.** Ensembles of seasonal volume transports through the strait for the 50 years of simulation. The volume transports for 1995–1996 from the model simulation and observations from *Sofianos et al.* [2002] are plotted. Also plotted are the transports averaged in 50 years and in 1980 from the model results.

Aiming to study the three-dimensional structure of the general circulation and its seasonal and interannual variability, we ran a high-resolution MITgcm (MIT general circulation model) [*Marshall et al.*, 1997] simulation for about 50 years, forced with high-frequency realistic atmospheric forcing. The seasonal variability of the overturning circulation is the focus of this two-part study, and the interannual variability of the overturning circulation throughout the 50 year long simulation will be explored in a forthcoming paper.

This study is divided into two parts. The first part is focused on the summer overturning and

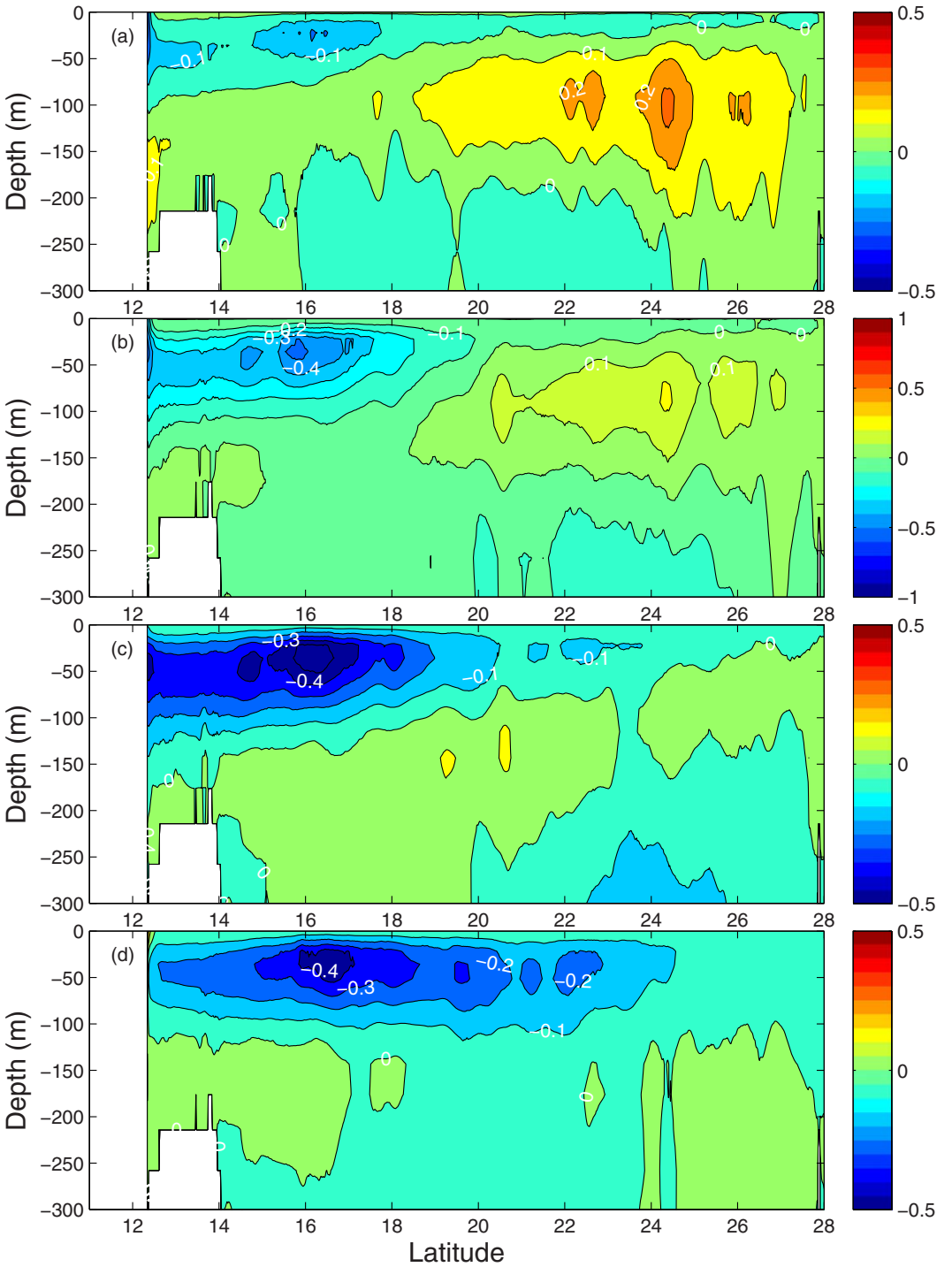


**Figure 4.** Development of the summer overturning circulation in the Red Sea. Stream functions (Sv) integrated across the basin are plotted for (a) June, (b) July, (c) August, and (d) September in 1980.

model validation, and the second part, presented in [*Yao et al.*, 2014], is focused on the winter overturning and its driving mechanisms. A recent joint KAUST/WHOI survey in September-October 2011 collected extensive hydrographic and current data along the eastern coast in the Red Sea north of 17°N. This survey provides detailed data regarding the structure of the intruding flow and is used as a benchmark to validate the summer model results. The rest of the paper is organized as follows. A brief description of the model configurations is given in section 2. In section 3, the model results of the vertical and spatial structure and the

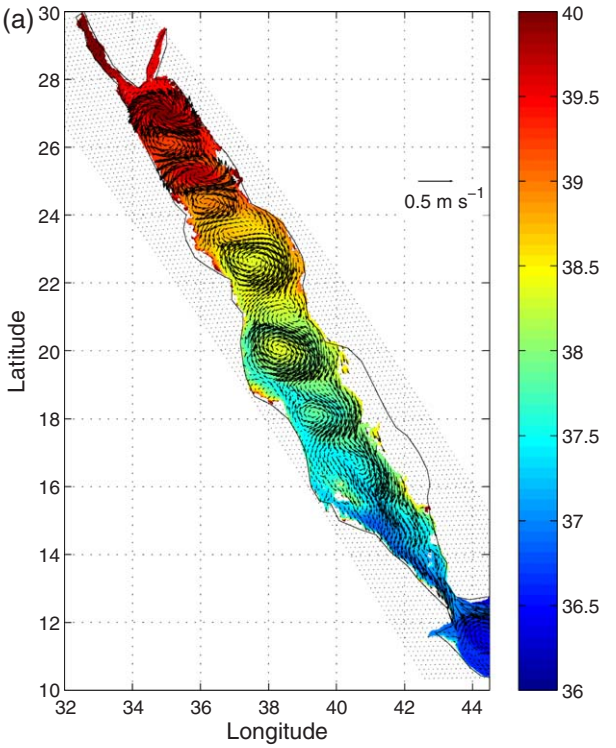


**Figure 5a.** Surface currents and salinity (psu) averaged from June to September in 1980. The blank region along the eastern coast between 16 and 18°N represents the shallow banks with complex bathymetry that are not well resolved in the model.

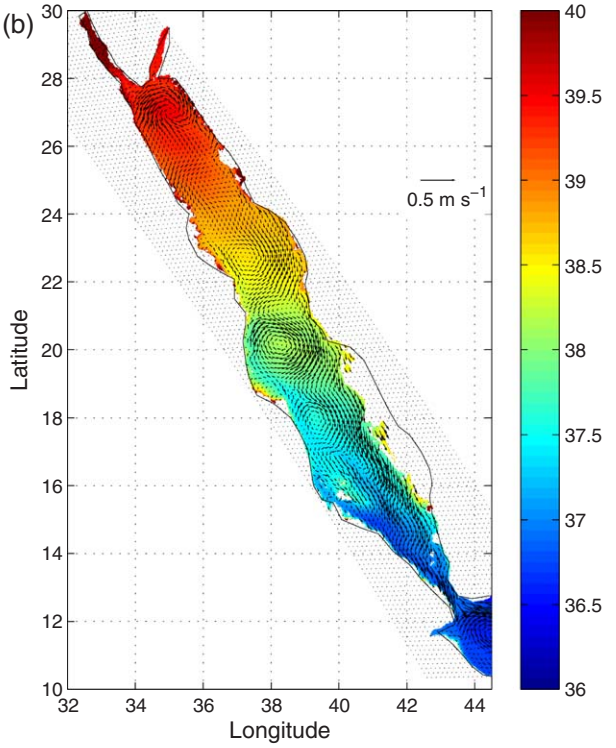


**Figure 5b.** Surface currents and salinity (psu) averaged from June to September for the climatological mean.

evolution of the summer overturning circulation is described and validated against available observations. In section 4, different forcing mechanisms of the summer intrusion, including the shoaling of the thermocline in the Gulf of Aden, surface wind stress in the Red Sea, surface heat flux, and hydraulics in the strait, are analyzed for the dynamical mechanisms of the summer reversal of the overturning circulation.

## 2. Model Configuration

The MITgcm is based on the primitive Navier-Stokes equations under the Boussinesq approximation. It is operated in this study in hydrostatic mode with an implicit free surface. Equations are written in $z$ coordinates and discretized using the centered second order finite differences approximation in a staggered "Arakawa C-grid." The model domain consists of the Red Sea, the Gulf of Aden, the Gulf of Suez, and the Gulf of Aqaba, with an eastern open boundary located at the Gulf of Aden (Figure 1). The model grids are defined on curvilinear coordinates rotated along the axis of the Red Sea, and in the following result description the along-basin and cross-basin velocities are referring to, respectively, the velocities in the direction along the axis and across the basin. The bathymetry of the basin is derived from the ETOPO2 data with corrections of depth at the Hanish Sill to 160 m according to *Sofianos et al.* [2002]. A shallower sill depth of 137 $\pm$ 3 m was identified for the Hanish Sill [*Lambeck et al.*, 2011]; however, since the deep part of the channel around the Hanish Sill is very narrow (~2 km) [see *Sofianos et al.*, 2002], the effect of the sill depth difference is considered minor in our model study of the general circulation in the Red Sea. The

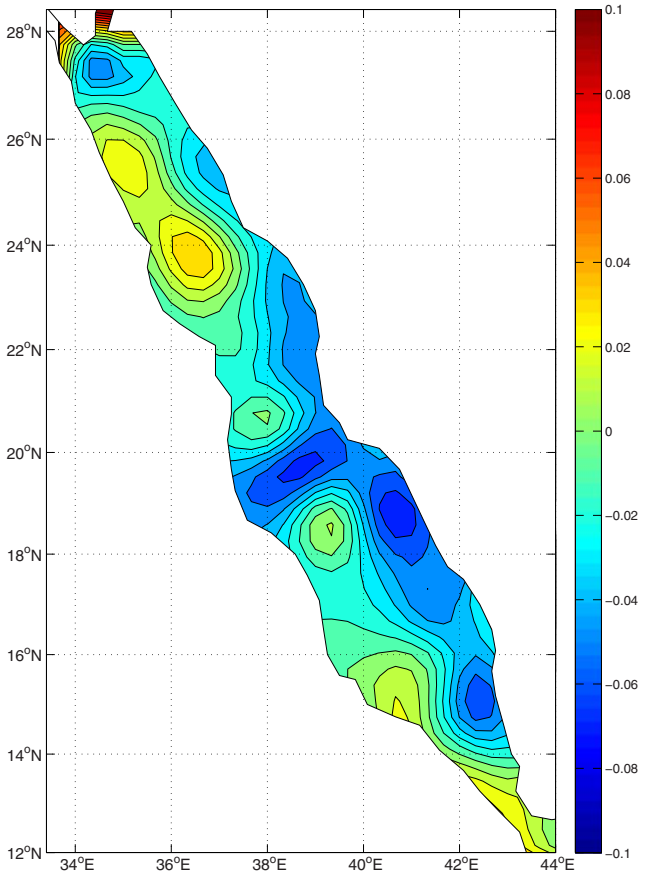


**Figure 6.** Sea surface height anomalies (m) in the Red Sea in August averaged from the AVISO data from 1993 to 2010.

average horizontal resolution is approximately 1.8 km, fine enough to resolve the narrow strait in the southern Red Sea. The resolution gradually increases to about 1.4 km in the north, which can resolve moderately the Strait of Tiran. The vertical grid is defined on 25 levels, whose depths increase from 10 m at the surface to 442 m near the bottom. The K-profile parameterization [*Large et al.*, 1994] is used for the vertical mixing scheme. The model is initialized with World Ocean Atlas 2001 [*Stephens et al.*, 2002; *Boyer et al.*, 2002], forced with the 6 hourly, NCEP reanalysis [*Kalnay et al.*, 1996] atmospheric data set with an approximate spatial resolution of 1.875° × 1.905°. The open boundary condition of temperature, salinity, and horizontal velocity components are specified with data from the Estimation of the Circulation and Climate of the Ocean (ECCO) project [*Köhl and Stammer*, 2008].

The MITgcm simulation used in this study differs from the previous modeling studies of the Red Sea by *Sofianos and Johns* [2002, 2003] in several important aspects, such as different vertical coordinate formulation (z level versus isopycnic), much higher horizontal resolution (∼1.8 km versus ∼10 km), realistic high-frequency forcing without correction to the atmospheric forcing, and realistic open boundary conditions.

After a 10 year spin-up run with the NCEP atmospheric forcing in 1952, a near 50 year simulation is followed from January 1952 to December 2001, during which the ECCO data are available for the open boundary conditions. Since our focus here is the seasonal variability, both results from a specific year and from climatological mean in all 50 years of simulation are analyzed. We choose the year 1980 at random to represent the seasonal circulation. Another experiment without the surface wind stress forcing is run from 1978 to 1981 to examine the direct role of the wind stress in the Red Sea, but the ECCO boundary conditions and the heat flux and freshwater flux are kept the same.

## 3. Model Results

### 3.1. Surface Wind Stress

The annual cycle of the monthly surface wind stress along the axis of the Red Sea for 1980 is shown in Figure 2. The seasonal pattern follows closely the climatological mean structure shown in *Sofianos and Johns* [2001]. During the winter monsoon months from October to May, the winds converge around 20°N in the Red Sea. In summer, the surface winds over the whole Red Sea are northwesterly in the whole basin. The heat flux and the fresh water flux over the surface of the Red Sea are presented in [*Yao et al.*, 2014] because they are the main atmospheric forcing in the winter overturning circulation.

### 3.2. Volume Transports Through the Strait

The seasonal exchange flow pattern through the strait, including the transition from the two-layer structure to the summer three-layer structure, is a robust feature in the 50 year run, even though some

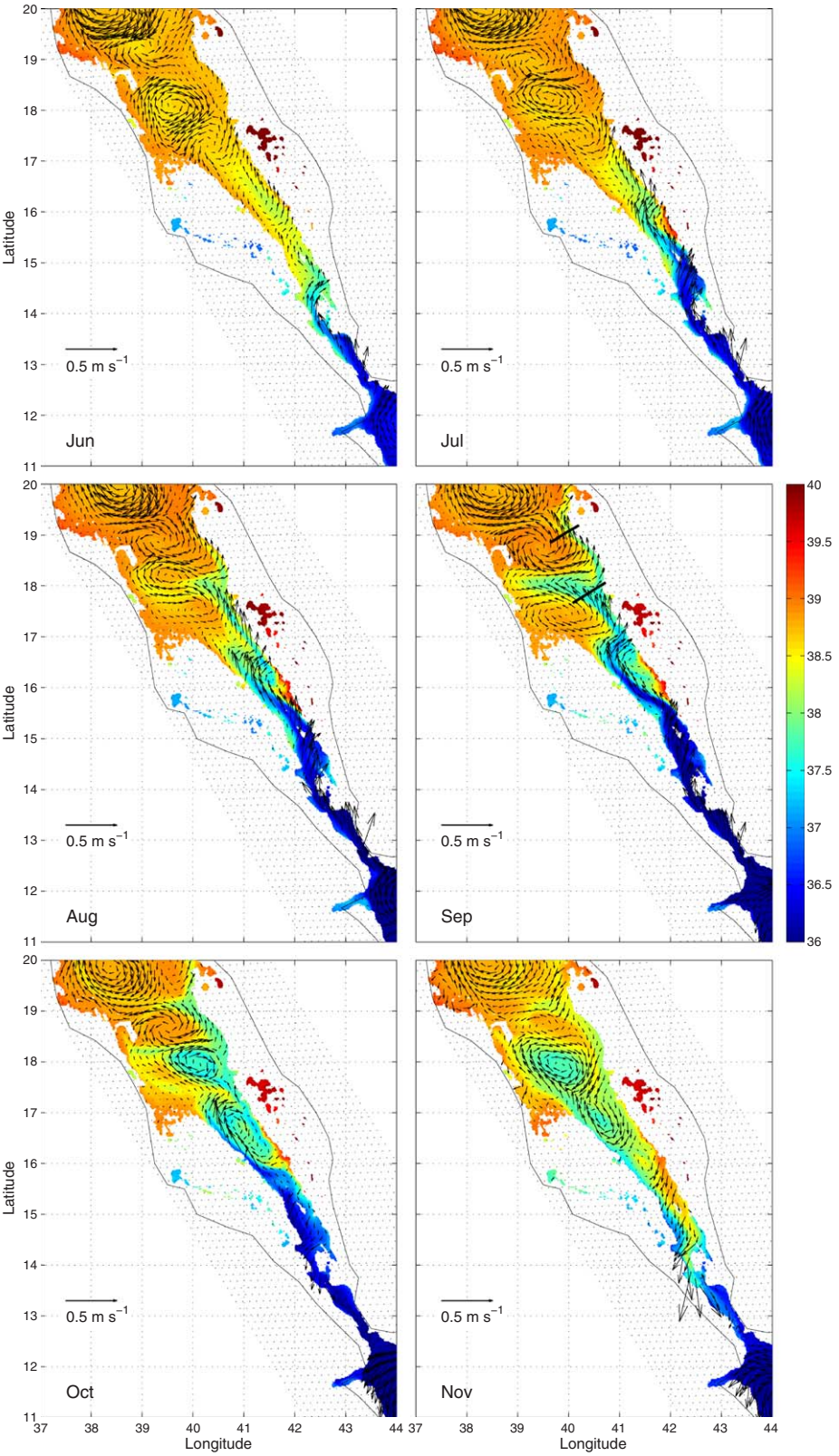


**Figure 7.** Currents and salinity (psu) at 80 m from June to November in 1980. The locations of the two observed transects are indicated by two lines in the plot for September.

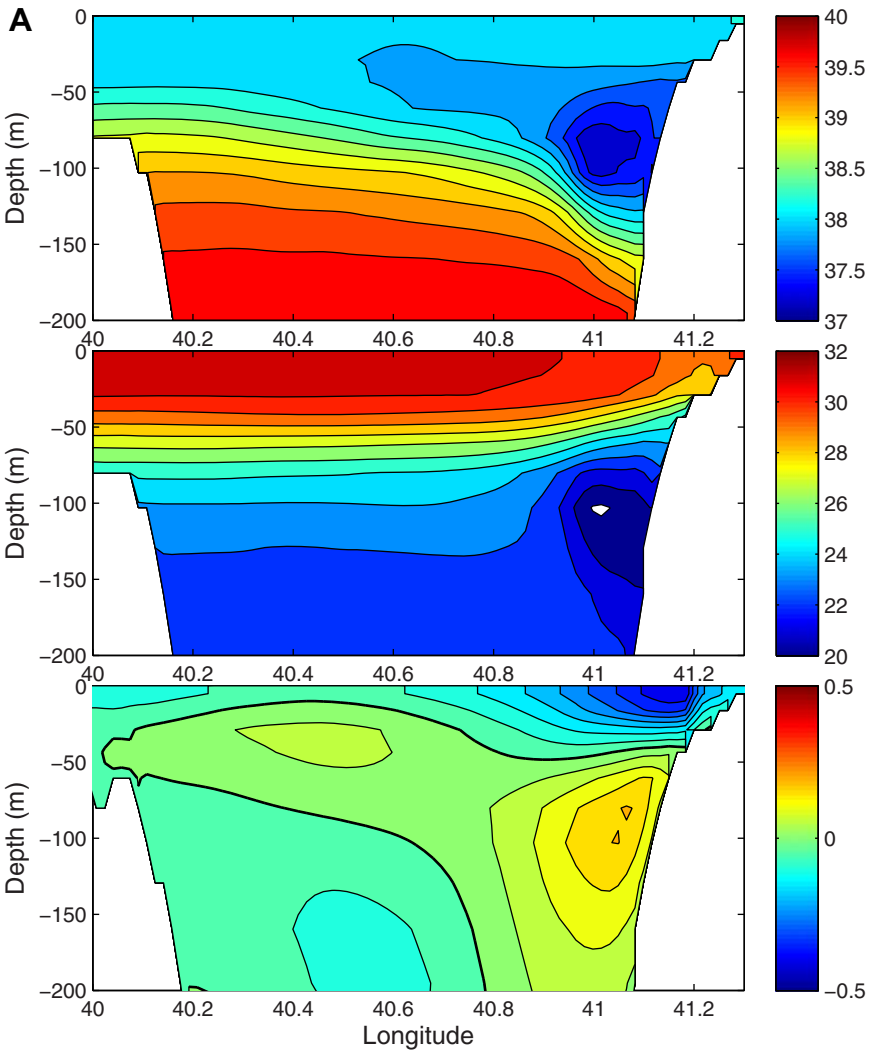


**Figure 8a.** Vertical sections of (top) salinity (psu), (middle) temperature (°C), and (bottom) cross-section velocity (m $s^{-1}$) at 17°N, from the model data averaged in September 1980.

interannual variability is also evident (Figure 3). The annual cycle of the volume transports of the surface water, GAIW, and RSOW in 1995–1996 compare very well with the observed results in the same period by *Sofianos et al*. [2002]. Compared with *Sofianos and Johns* [2002] model results, the amplitudes and phases of the exchange flows are in better agreement with the observations, particularly the weak summer RSOW. The volume transports in 1980 have an overall similar shape to the mean transports, and this justifies the use of the result in 1980 to give a representative description of the annual cycle of the seasonal overturning circulation.

### 3.3. Development of the Summer Overturning Circulation

As discussed in detail in [*Yao et al.*, 2014], during the months from October to May, the winter-type overturning circulation in the Red Sea is present. From June to September, the overturning circulation in the Red Sea that drives the water exchange in the strait is reversed from the winter overturning circulation and consists of a surface outflow and a subsurface inflow that upwells inside the basin. Due to the elongated shape of the Red Sea, the overturning circulation structures are readily represented by stream functions, which are obtained by integrating the along-basin volume transports across the basin. The monthly mean stream function as a function of depth and latitude from June to September are shown in Figure 4. The summer overturning cell is first established in the upper 120 m in the southern basin in June, while the winter overturning cell retreats to the north and to deeper depths. The summer overturning cell extends

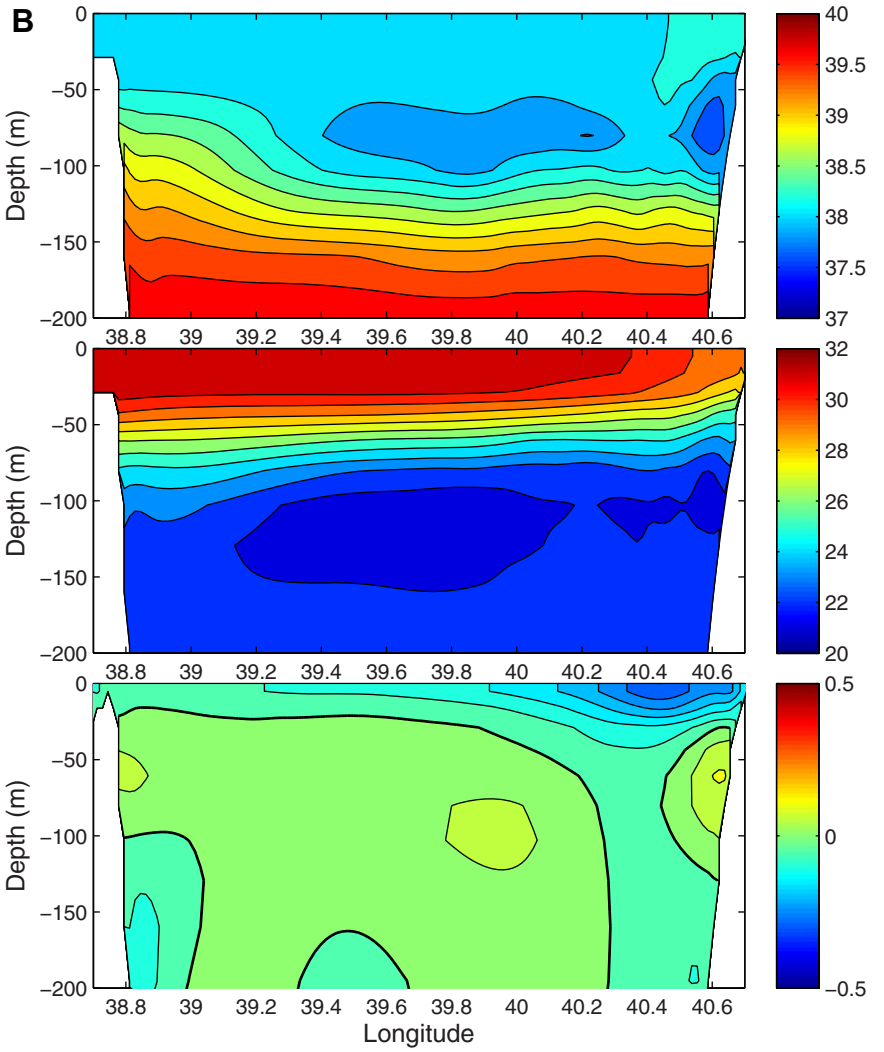


**Figure 8b.** Vertical sections of (top) salinity (psu), (middle) temperature (°C), and (bottom) cross-section velocity (m $s^{-1}$) at 18°N, from the model data averaged in September 1980.

gradually toward the north and reaches 24°N in September, when the winter overturning cell diminishes almost completely. The maximum overturning rate of 0.5 Sv occurs around 16°N in August.

### 3.4. Summer Surface Circulation

The surface currents superimposed on the salinity field averaged from June to September from the 1980 model results are presented in Figure 5a. The surface current field is characterized by a chain of alternating cyclonic and anticyclonic eddies, which appears to be more energetic than the summer model results in *Sofianos and Johns* [2003]. These eddies are associated with much stronger currents than the overturning circulation, with speed as fast as 0.5 m $s^{-1}$. It is interesting to note that the eddies north of 24°N are dominated by cyclones located around 25°N and 27°N, respectively, whereas the eddies south of 24°N are dominated by anticyclones located around 18°N, 20°N, and 23°N, respectively. The anticyclonic features in the southern Red Sea are consistent with the observational results in *Sofianos and Johns* [2007] and *Quadfasel and Baudner* [1993]. In a summer synoptic survey in 2001, *Sofianos and Johns* [2007] identified three anticyclonic eddies located at 23°N, 21.2°N, and 18.6°N. In *Quadfasel and Baudner* [1993], depressions of the isotherms from hydrographic data suggest the locations of a permanent eddy around 23°N, and two seasonal eddies around 20–21°N, and 17–18°N, respectively. In fact, these eddies appear to be persistent in summers as suggested by the climatologically averaged surface current fields in Figure 5b. The summer sea surface height anomalies averaged from the merged altimetric AVISO

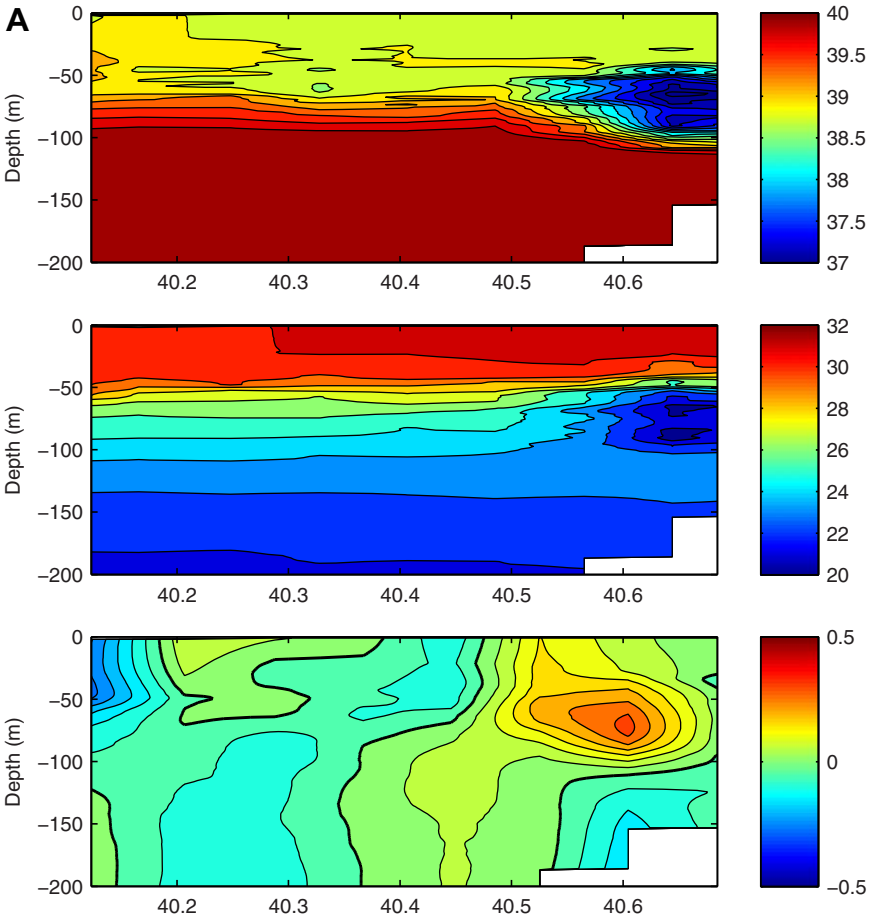


**Figure 9a.** Vertical sections of (top) salinity (psu), (middle) temperature (°C), and (bottom) cross-section velocity (m $s^{-1}$) from the observations in 2011 for the southern section shown in Figure 6.

1993–2010 data are shown in Figure 6. The locations of the anticyclonic eddies associated with the local sea surface height maxima correspond well with their locations in Figures 5a and 5b. The cyclonic eddy around 27°N in the model is also observed in the altimetry data.

The summer surface salinity in the Red Sea in 1980 increases from about 36 psu around the strait to about 40 psu in the northern part of the Red Sea. It has a similar spatial structure to that in winter [*Yao et al.*, 2014], except that the summer surface salinity is higher in the southern basin. The surface outflow carrying relatively salty waters becomes evident only in the southern Red Sea and tends to intensify against the eastern coast (Figure 5a).

### 3.5. Intrusion of the Gulf of Aden Intermediate Water

The inflow in the intermediate depth in the summer overturning circulation is supplied by the GAIW. The summer observations (south of 17°N) in *Sofianos and Johns* [2007] reveal a complex three-dimensional structure of the intruding flow in the southern Red Sea. To describe the full cycle of the three-dimensional structure of propagation and fade of the GAIW inside the basin, the current and salinity fields at 80 m from the model from June to November are plotted in Figure 7, and the vertical sections for September along approximately 17°N and 18°N are plotted in Figure 8. To compare the model results against observations, two relevant section plots based on the 2011 survey data are presented in Figure 9. The locations of the observed sections are shown in Figure 7. The spreading pathways for the GAIW for 1980 and the climatological mean model results are further investigated on the density surface in Figure 10.

The model shows that from June to September, low-salinity water enters the Red Sea through the strait as a strong subsurface inflow with speed about 0.5 m $s^{-1}$ (Figure 7). As it moves to the north,

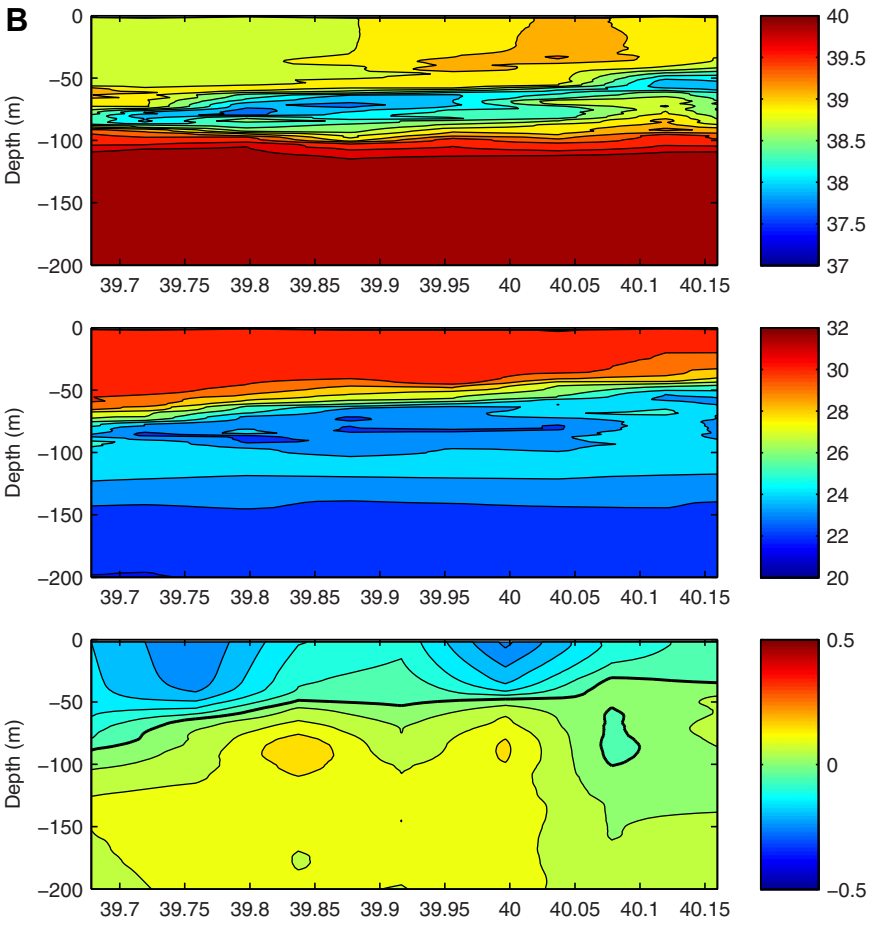


**Figure 9b.** Vertical sections of (top) salinity (psu), (middle) temperature (°C), and (bottom) cross-section velocity (m $s^{-1}$) from the observations in 2011 for the northern section shown in Figure 6.

the intruding GAIW tends to be banked against the eastern coast but is diverted to the interior of the basin because of its interaction with two anticyclonic eddies centered at about 16.5°N and 18°N, respectively, since August. In September, most of the low-salinity water is diverted into the west at 18°N, and a small portion of the inflow propagates farther northward along the eastern coast. During October and November, when the subsurface flow in the strait is reversed, most of the GAIW is trapped inside the eddy located at 18°N and the entire basin south of it, and the low-salinity signal is gradually weakened by lateral mixing (Figure 7).

The availability of the model data for 1952–2001 prevents direct comparison with the 2011 observation for the same year. Nonetheless, as shown later in the climatological mean (Figure 10b), the GAIW intrusion in the Red Sea exhibits a persistent seasonal structure, and the vertical structure of the intruding GAIW in the southern Red Sea between the 1980 model results and the 2011 observations shows a strong correspondence. In the observed transect around 17°N, a well-defined core of GAIW with temperature of about 20°C and salinity of 37 psu is located between the depths of 50 and 100 m, banked against the eastern coast in a narrow band with a width of about 20 km (Figure 9a). The model results at 17°N show a very similar structure of the GAIW except that, for the monthly mean value, the core is wider and deeper, extending down to 200 m. The lateral spreading of the GAIW into the interior by eddies is present in both the observations and model results, although not at the exact same locations. In the observation, the GAIW is stirred laterally and is manifested as a thin layer with temperature around 24°C and salinity around 38 psu between the depths of 50 and 100 m (Figure 9b). The model result for the section at 18°N also captures this feature with similar distributions of temperature, salinity, and velocity (Figure 8b). The thermoclines are tilted upward at the eastern coast both in the model and in the observations. This is consistent with upwelling along the eastern coast driven by the summer surface northwesterly winds over the southern Red Sea. This also suggests the

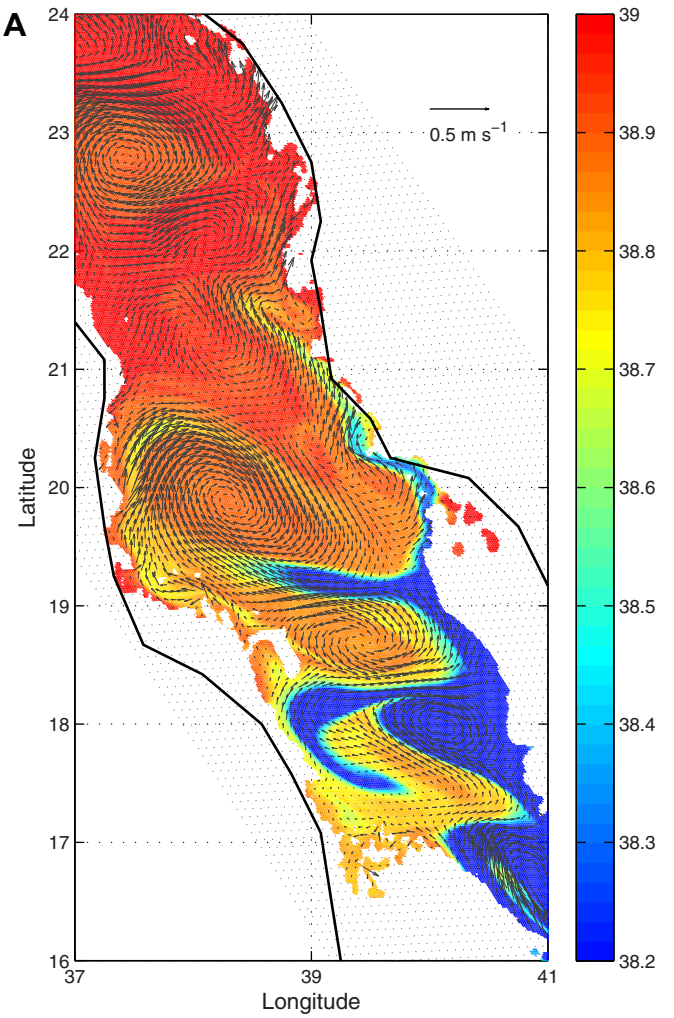


**Figure 10a.** Currents and salinity (psu) on the density surface $\sigma = 26.1$ for the model results on 30 September 1980.

intermediate intruding GAIW upwells along the eastern coast and may supply the southward surface branch in the summer overturning circulation as shown in Figure 4.

Because the core of the intermediate intruding flow shoals toward the north as indicated by the overturning stream functions in Figure 4, the spreading of the GAIW in the Red Sea is more accurately examined by water properties on density surface. By the end of September, the salinity on the density surface $\sigma = 26.1$, where the minimum salinities are located, suggests the intermediate low-salinity water reaches north of 22°N along the eastern coast as an unstable filament and then loses its salinity characteristics quickly, mainly due to lateral mixing (Figure 10a). The overturning circulation in Figure 4 suggests the boundary current associated with the inflow can penetrate to 24°N in September, much farther north than the latitude of 18°N as suggested in the observation in *Maillard and Soliman* [1986].

The climatological mean distributions of salinities and currents on $\sigma = 26.1$ as shown in Figure 10b confirm that the spreading of the GAIW in the Red Sea over the 50 year simulation is controlled by two processes. First, the persistent inflow advects the GAIW northward along the eastern boundary. Although the GAIW is not clearly distinguishable from the ambient water north of 21°N in the Red Sea, the eastern boundary current extends north of 24°N. This is in agreement with the 2011 summer observations (J. Churchill et al., The transport of nutrient-rich Indian Ocean water through the Red Sea and into coastal reef systems, submitted to *Journal of Marine Research*, 2013), in which a subsurface northward flow extending up to 24°N at the depths 50–80 m was observed along the eastern coast. Second, the unstable eddies south of 18°N, even though without showing persistent mean structures, transport significantly low-salinity GAIW into the interior of the Red Sea.

## 4. Forcing Mechanisms of the Summer Intrusion

Because of the coincidence between the reversal of the surface winds in the southern Red Sea and the Gulf of Aden and the reversal of the overturning circulation, the forcing mechanisms of the summer overturning circulation in the Red Sea are generally associated with the seasonal Indian monsoon system. However, the detailed mechanisms involved remain disputable.

*Patzert* [1974] argues that upwelling in the Gulf of Aden, driven by westerly winds, is the primary reason for the reversal of the summer circulation, due to the creation of a reversed pressure gradient at intermediate

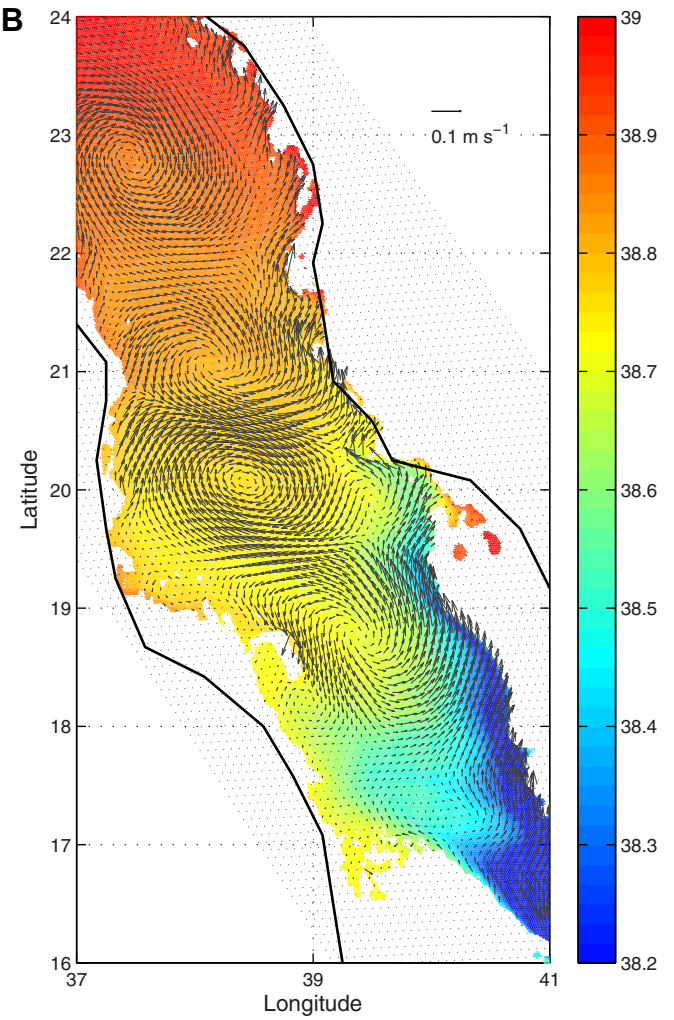


**Figure 10b.** Currents and salinity (psu) on the density surface $\sigma = 26.1$ for September in the climatological mean.

depths. In a numerical study with a global grid, *Aiki et al*. [2006] find that remote surface wind acting broadly over the Arabian Sea, and not just in the Gulf of Aden, control the shoaling of the thermocline in the Gulf of Aden. *Sofianos and Johns* [2002] in a modeling study conclude that both the direct and indirect effects of the surface winds are important in driving the summer circulation. Using a hydraulic model driven only by the shoaling of the thermocline in the Gulf of Aden, *Siddall et al*. [2002] is able to produce the intermediate intrusion in summer, suggesting a minor direct effect of the surface wind.

As discussed later in this section, the direct and indirect wind stress forcing is insufficient to explain the timing of the intrusion in summer. The vertical density structure changes in the upper layer resulting from the latitudinal heating difference between the Gulf of Aden and the Red Sea and the salinity increase from the reversed surface currents in the southern basin are also important factors. *Siddall et al*. [2002] also shows that the surface temperature (and therefore the density) acts as a factor controlling the exchange flux in the strait.

The exchange flow through the narrow strait, particularly around the Hanish Sill and Perim Narrows, could be also limited by hydraulic control if the exchange flows reach the critical speeds. The above various controlling mechanisms for the summer overturning circulation are examined in this section from the model results in 1980.

### 4.1. Momentum Balance

In order to investigate the dynamical processes that drive the summer overturning circulation, the along-basin momentum balances in the Red Sea are examined. The along-basin momentum equation in a coordinate rotated along the axis of the Red Sea,

$$v_t = -p_y/\rho - fu - (uv_x + vv_y + wv_z) + (A_h v_{xx} + A_h v_{yy}) + (A_z v_z)_z, \quad (1)$$

states that the time rate of change of the meridional velocity is governed by the summed of the right side terms, including the pressure gradient force, Coriolis force, advection, horizontal viscosity, and vertical viscosity. Each term in the above equation can be directly diagnosed from the model results. To obtain a relatively steady relation for the momentum balance in the overturning circulation, the momentum equation is integrated spatially across the basin and along the basin for different regions in the basin and temporally for a period of one month. In the integrated form, the surface wind stress is included in the vertical viscosity

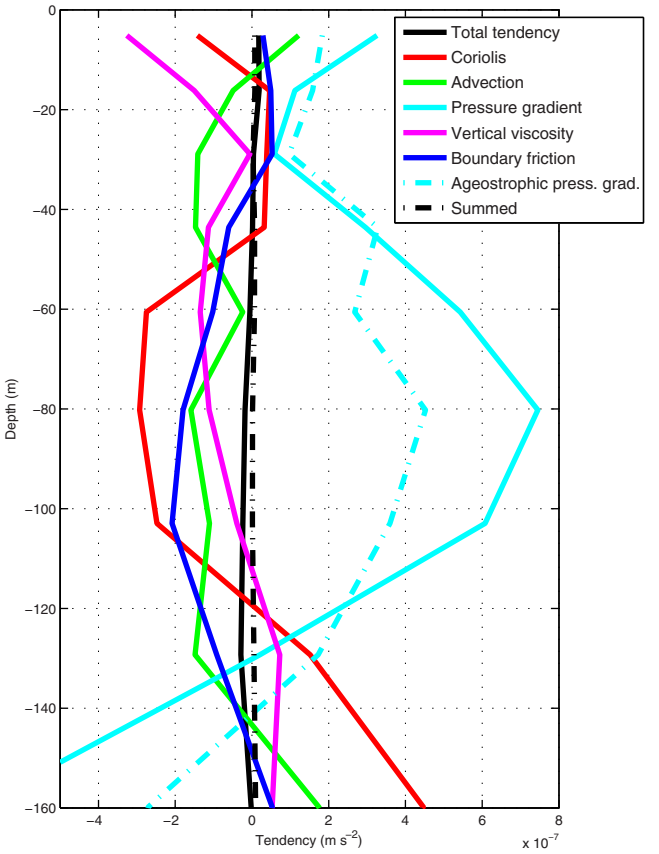


**Figure 11a.** Along-strait momentum balance diagnosed from the model for August 1980 in the strait.

term, and the lateral friction horizontally integrated from the horizontal viscosity term and the explicit bottom drag are together referred to as the boundary friction term.

The vertical profiles of each term integrated along the strait from 12.5°N to 14.6°N are plotted in Figure 11a. The profile of the summed terms from the right side of the equation falls close to the total tendency term diagnosed directly from the model, and the relatively small magnitude of difference confirms the near-steady balance. Because the cross-channel velocity in the strait is limited, the Coriolis force in the strait is only moderately strong at middepth. The ageostrophic along-channel pressure gradient is obtained by removing the Coriolis force from the total pressure gradient term and is also plotted in the figure. In the top layer, the surface wind stress penetrates the upper 30 m and is balanced by the pressure gradient force toward the Red Sea, which, as shown in Figure 14, is caused by the surface slope tilting downward northward. In the depths 50–130 m, a strong pressure gradient force is established northward, with the maximum value occurring at around 80 m

Both the vertical viscosity and boundary friction are similarly important in balancing the subsurface pressure gradient force in the strait. The vertical viscosity has a relative maximum around 60 m where the interface of the inflow and outflow, and hence the maximum vertical shear is located (Figure 17). This suggests the important role of the vertical mixing. The maximum boundary friction takes place around 80–100 m, corresponding to the position of the core of the intruding GAIW (see Figure 16). This suggests that the side drag in the narrow strait is an important source of friction. In contrast, *Smeed* [2000] and *Biton et al.* [2008] considered the effect of the vertical mixing in the hydraulic models and showed a minor contribution of vertical mixing for the water exchange in the strait. This discrepancy is probably due to the different representations of vertical mixing in the models.

The momentum balance in the southern basin is shown in Figure 11b, where the vertical profiles of the tendency terms integrated between 18°N and 20°N are plotted. The dominant balance inside the basin is between the Coriolis force and the pressure gradient force due to strong cross-basin currents. Secondarily, the surface wind stress in the upper 40 m is balanced by the pressure gradient force resulted from the surface slope and density gradient that increases to the north (see Figure 14). The rest of the terms are much less significant at all depths. The momentum profiles for other central and northern regions in Red Sea show basically similar balances.

### 4.2. Shoaling of the Thermocline in the Gulf of Aden

The shoaling of the thermocline during summer is traditionally considered to be a local response to the southwesterly winds in the Gulf of Aden and to be confined to the northern coast [e.g., *Patzert*, 1974].

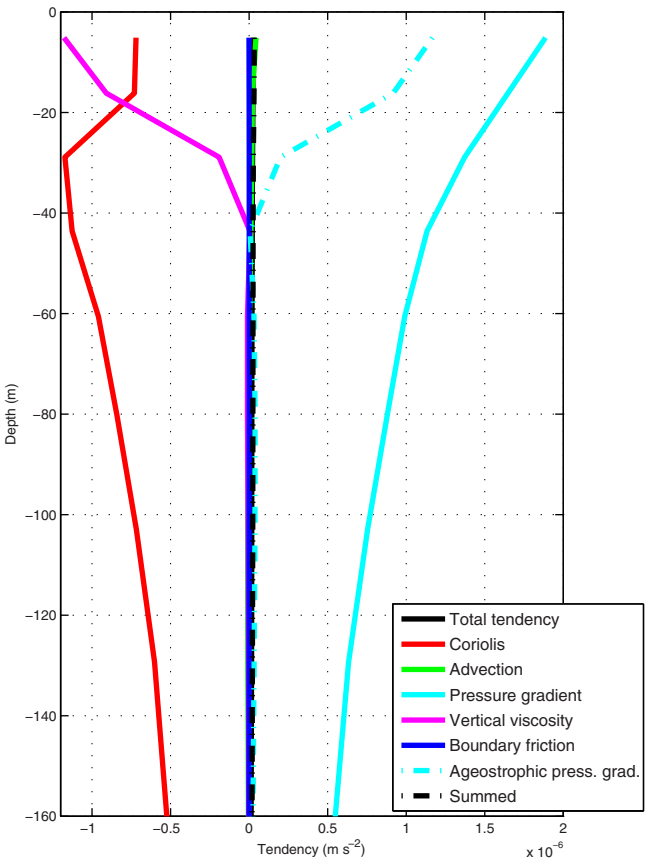


**Figure 11b.** Along-basin momentum balance diagnosed from the model for August 1980 in the southern Red Sea.

However, in a recent modeling study by *Aiki et al.* [2006], it is suggested that the meridional component of the surface wind stress at the eastern boundary of the Gulf of Aden drives a surface outflow associated with Ekman transport. This surface outflow determines the shoaling of the thermocline in the Gulf of Aden and the seasonal exchange through the strait. Relatively, high-resolution observational data in *Bower and Furey* [2012] show that the thermocline in summer is uplifted by about 50 m in the entire Gulf of Aden except some smaller scale perturbations associated with eddies.

Figure 12 shows the annual cycle of the thermocline depth represented by the 20°C isotherm averaged in the Gulf of Aden for 1980 in the experiment with full forcing. The effect of the coastal upwelling on the thermocline depth is indicated by the 20°C isotherm averaged for the area north of 12°N. The thermocline in the entire Gulf of Aden is displaced upward from May, reaches the shallowest depth in August, and falls back to the winter depth in December. The thermocline depth for the coastal area north of 12°N is slightly shallower but with a similar seasonal pattern, suggesting the less significant effect of the coastal upwelling on the thermocline depth even for the coast. The thermocline depth in the model is for some unknown reason deeper than that shown in *Bower and Furey* [2012]. In the experiment with buoyancy forcing only (not shown here), the annual cycle of the thermocline shows a very similar temporal and vertical structure. This indicates that the thermocline in the Gulf of Aden in the model is mostly driven by the open boundary conditions from ECCO, which is consistent with the findings in *Aiki et al.* [2006].

In the experiment with buoyancy forcing only, the shoaled thermocline in the Gulf of Aden establishes a reversed pressure gradient at the intermediate depth, which drives a summer reversed exchange through the strait from June to September but with significantly weaker subsurface inflows (Figure 13). The mean intrusion rate is reduced from 0.31 Sv in the experiment with full forcing to 0.21 Sv (Figure 14). Compared with Figure 7, the weaker intrusion in Figure 13 can only reach approximately 17°N in September before losing its distinct water properties.

### 4.3. Surface Wind Stress in the Red Sea

The surface winds in the Red Sea significantly enhance the reversed summer water exchanges in the strait and the intrusion of the GAIW as suggested in Figures 7, 13, and 14. As shown in the momentum balance analysis, the surface wind stress only penetrates to the top 30–40 m approximately, and this raises the question of how the winds increase the subsurface intrusion? The volume transport in the strait, pressure difference at 80 m, and sea surface height difference between the Gulf of Aden (averaged around 12°N) and the Red Sea (averaged around 18°N) for experiments with and without surface winds are compared in Figure 14. The volume transports of GAIW are closely related to the pressure differences both in magnitude and in phase.

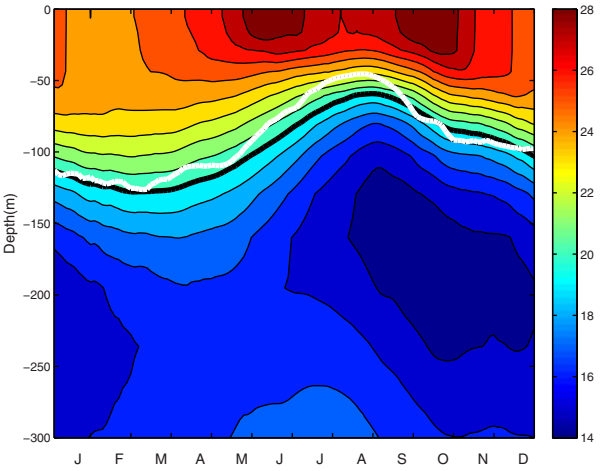


**Figure 12.** Annual cycle of the thermocline depth represented by the 20°C isotherm (the thick contour line) in the Gulf of Aden in 1980 in the experiment with full forcing. The 20°C isotherm for the area north of 12°N in the Gulf of Aden is indicated by the white line.

Figure 14 suggests that the sea surface height difference in summer indicates a surface downward slope toward the northern Red Sea and hence a barotropic pressure gradient force northward toward the Red Sea. In the surface layer, this pressure gradient force is balanced by the surface wind stress (Figures 11a and 11b), which is consistent with the findings from an analysis of the altimetry data and the wind stress data in the Red Sea by *Sofianos and Johns* [2001]. The barotropic pressure gradient caused by the surface wind stress contributes to increase the subsurface pressure gradient, adding to the baroclinic pressure difference caused by the shoaling of the thermocline, therefore, increasing the strength of the subsurface intrusion in summer (Figure 15).

### 4.4. Vertical Density Structure Changes in the Upper Layer

Comparison of Figures 12 and 14 shows that the cycle of the subsurface intrusion and pressure difference are not aligned with the annual cycle of the thermocline depth in the Gulf of Aden. The intrusion occurs from June through September, while the thermocline stays uplifted above the pre-June level till December. Since the intrusion without surface wind stress forcing follows a similar cycle with decreased amplitudes, it cannot be explained by the cycle of the summer surface wind stress.

To explore additional controlling mechanisms for the reversal of the intermediate water in October, the water properties for August and October in the upper layer in the Gulf of Aden and in the Red Sea are examined in Figure 16, where vertical profiles averaged around 12°N and averaged around 18°N, respectively, are displayed. The temperature in the upper 80 m in the Gulf of Aden undergoes marked warming by about 1.5°C from August to October, which is also indicated in Figure 12. Meanwhile, the salinities also show only a slight increase. As a result, the water in the upper 80 m in the Gulf of Aden becomes less dense from August to October. In contrast, the water in the upper 80 m in Red Sea undergoes a general salinity increase with maximum values of about 0.5 psu occurring at the surface, while the temperatures remain relatively constant from August to October. The density in the Red Sea in the upper 44 m increases slightly from August to October (Figure 16a). The changes of water properties in the upper layer in the Gulf of Aden and the Red Sea leads to the reversal of the density difference and pressure difference (Figures 16b and 16c). In August, the water in the upper 60 m in the Gulf of Aden is denser than that in the Red Sea, and this contributes to a northward pressure gradient for the upper 100 m. In October, the changes of water properties in the upper layers reverses the density difference and hence the pressure gradient and reversal of the intrusion of the intermediate water.

These changes of water properties from August to October can be explained by two processes. First, owing to the seasonal solar path in the Red Sea region, the summer heat flux from the solar insolation in the southern Red Sea and the Gulf of Aden has a complex temporal and spatial variation that can affect the summer overturning circulation. For instance, during July and August the central Red Sea receives more insolation than the Gulf of Aden, while during September the Gulf of Aden has a larger heat gain for shortwave radiation than in the southern Red Sea. This results in two separate surface temperature maxima in June and October in the Gulf of Aden. The higher temperatures, particularly in October, reduce the density in the upper layer in the Gulf of Aden as shown in Figure 16a. Second, the reversal of the winter overturning circulation in early summer stops the supply of relatively fresh water from the Gulf of Aden for the upper layer in the Red Sea, and at the same time the surface salinity in the southern Red Sea is increased by the southward surface current that advects relative more salty water from the northern Red Sea (Figure 5a).

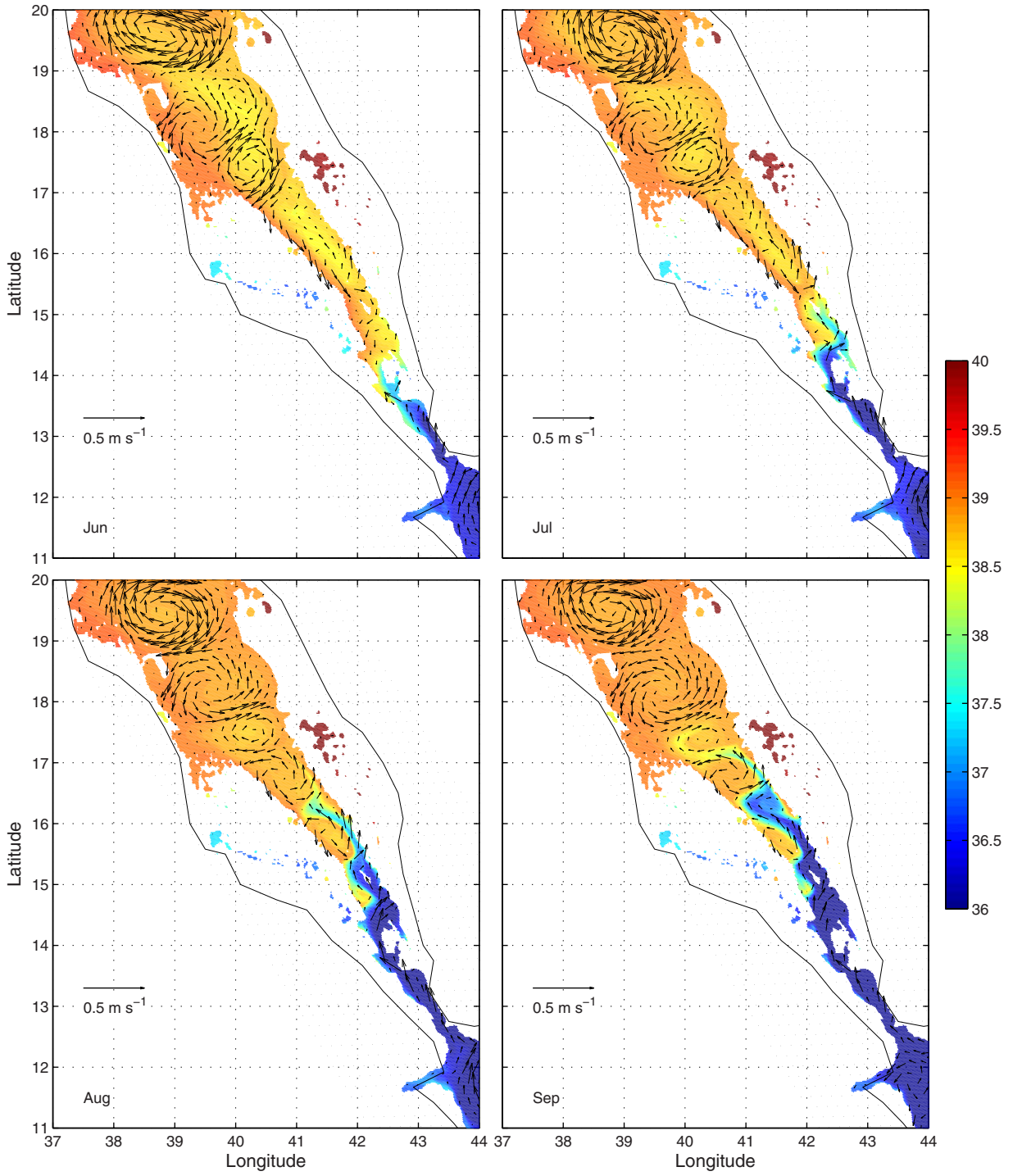


**Figure 13.** Currents and salinity (psu) at 80 m for (a) June, (b) July, (c) August, and (d) September in 1980 for the experiment without wind forcing.

### 4.5. Hydraulics in the Strait

An unsettled question concerning the exchange between the Red Sea and Gulf of Aden is whether this exchange is hydraulically controlled. Certainly the Perim Narrows and Hanish Sill are constrictions that could potentially exert hydraulic control and thereby limit the information that can pass into the Red Sea from outside due to long internal gravity waves. This issue, which speaks to the degree to which the physical

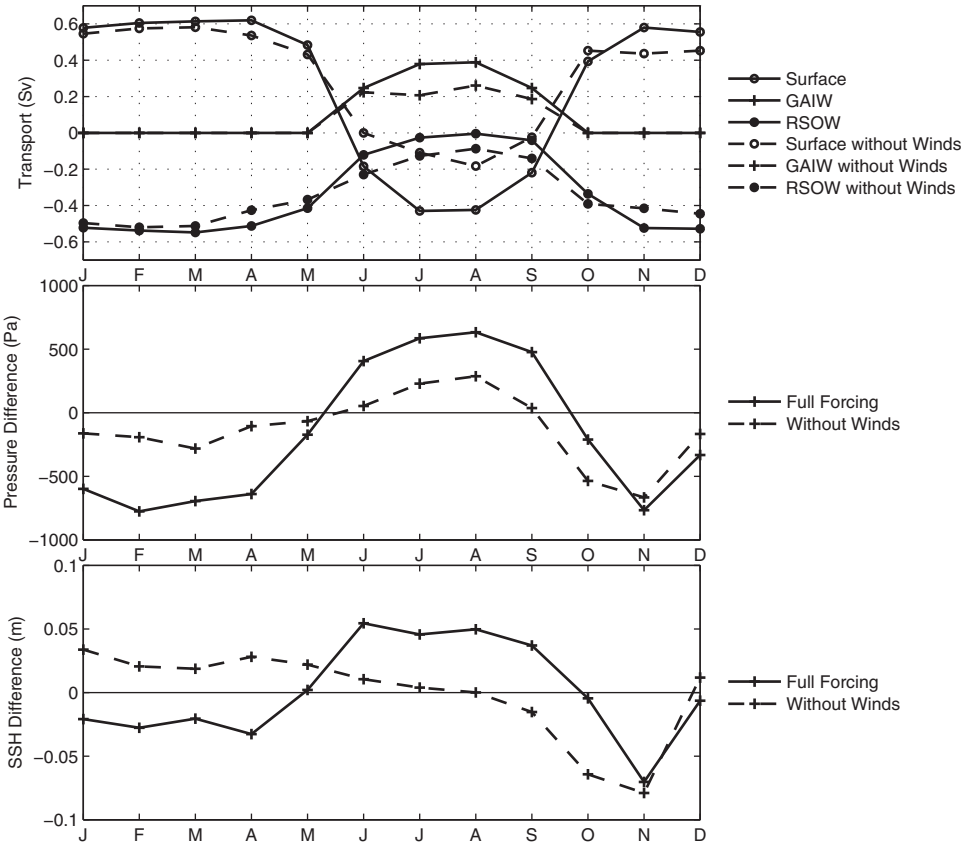


**Figure 14.** Annual cycles of water exchange through (top) the strait, (middle) pressure difference at 80 m, and (bottom) sea surface height (SSH) difference between the Gulf of Aden (averaged around 12°N) and the Red Sea (averaged around 18°N) in 1980.

properties of the Red Sea are locally determined, is complicated by the seasonal reversal of the exchange flows and the transition from a two-layer exchange structure in winter months (October-May) to a three-layer exchange structure in summer months (June-September) (Figure 3).

For a two-layer exchange flow in a channel with a rectangular section and no transverse variation, there are two internal long waves, each corresponding to a first baroclinic mode. The critical condition is reached when the composite Froude number $G^2$ is unity

$$G^2 = F_1^2 + F_2^2 = 1, \tag{2}$$

where $F_i (i = 1, 2)$ is the Froude number for layer $i$. The flow is supercritical when $G^2 > 1$, meaning that the layer velocities are sufficiently strong that the two waves propagate in the same direction. In the most likely controlled setting, the two waves would propagate toward the Gulf of Aden, and thus the information flow would be in one direction. For the three-layer exchange flows in the strait, two internal wave modes, each associated with two waves, are present, and the critical conditions are more complicated. *Smeed* [2000] derives the critical condition for a three-layer model with rectangular cross section and uses this model to simulate the response of the exchange flows to the seasonal variation of the thermocline depth in the Gulf of Aden.

Based on the measurements by *Murray and Johns* [1997], *Pratt et al.* [1999, 2000] found that the monthly mean summer flow at the Hanish Sill and the Perim Narrows is subcritical with respect to the first and second internal modes. This conclusion was based on the computation of modes from both a three-layer system and a system with continuously varying velocity and stratification. However, the data were only available at the sill and narrows, and the cross-channel shear of the horizontal velocity was neglected in their studies. The authors note that friction could shift the control point away from the sill or narrows.

The critical condition of the exchange flows that takes account the cross-channel variation of horizontal velocity within each layer is derived by *Pratt* [2008]. For two-layer flows, the critical condition can be expressed as

$$G_w^2 = \frac{1}{\frac{1}{w_{12}}\int_{x_{L1}}^{x_{R1}} \frac{g'_{21}D_1}{V_1^2}dx} + \frac{1}{\frac{1}{w_{12}}\int_{x_{L2}}^{x_{R2}} \frac{g'_{21}D_2}{V_2^2}dx} = 1, \tag{3}$$

and for three-layer flows, the critical condition is

$$\tilde{F}_1^2 + \left(\frac{1-r}{r} + \frac{w_{23}}{w_{12}}\right)\tilde{F}_2^2 + \tilde{F}_3^2 - \frac{w_{23}}{w_{12}}\tilde{F}_1^2\,\tilde{F}_2^2 - \tilde{F}_1^2\,\tilde{F}_3^2 - \frac{1-r}{r}\tilde{F}_2^2\,\tilde{F}_3^2 = 1, \tag{4}$$

where

$$\tilde{F}_1^2 = \left(\frac{1}{w_{12}}\int_{x_{L1}}^{x_{R1}} \frac{g'_{21}D_1}{V_1^2}dx\right)^{-1},$$
$$\tilde{F}_2^2 = \left(\frac{1}{w_{23}}\int_{x_{L2}}^{x_{R2}} \frac{g'_{32}D_2}{V_2^2}dx\right)^{-1},$$
$$\tilde{F}_3^2 = \left(\frac{1}{w_{23}}\int_{x_{L3}}^{x_{R3}} \frac{g'_{32}D_3}{V_3^2}dx\right)^{-1},$$

$w_{12}$ and $w_{23}$ are the width of the interface between the first and the second layer, and the second and the third layer (if exists), respectively. Also, $x_{Li}$ and $x_{Ri}$ $(i=1,2,3)$ are, respectively, the left and right boundary locations in the transverse direction of each layer, $D_i(i=1,2,3)$ is the depth of each layer (each assumed constant), $V_i(i=1,2,3)$ is the velocity of the flow in each layer, $g'_{21}=g(\rho_2-\rho_1)/\bar{\rho}$, $g'_{31}=g(\rho_3-\rho_1)/\bar{\rho}$, $g'_{32}=g(\rho_3-\rho_2)/\bar{\rho}$, with $\rho_i(i=1,2,3)$ being the density for each layer, $\bar{\rho}$ the mean density, and $g$ the gravitational acceleration, and $r=(\rho_2-\rho_1)/(\rho_3-\rho_1)$. The parameters $\tilde{F}_1^2$, $\tilde{F}_2^2$, and $\tilde{F}_3^2$ can interpreted as generalized layer Froude numbers.

As suggested by the volume transports in Figure 3, the three-layer exchange structures, hence the hydraulics, in the strait are constantly evolving during the summer overturning circulation from June to September. The exchange structures in the model along the strait for June and August are shown in Figures 17 and 18, respectively, with the former representing the stage when the two-layer winter exchange structure has just transitioned to the three-layer exchange flows and the latter representing the stage when the summer subsurface intrusion peaks. The temperature, salinity, density, and along-channel velocity averaged across the strait, together with the layer Froude numbers for each layer, calculated with equation (4), are plotted in these figures. During June, a relatively cold and fresh water tongue below 50 m shows up in the southern entrance of the strait, and the relatively warm and salty deep waters associated with the deep outflow is suppressed there (Figure 17). In contrast to the limited presence of the relatively cold and fresh intruding water, the subsurface inflow is fully established in the whole strait and in the southern Red Sea, and the surface flow is reversed from the winter direction.

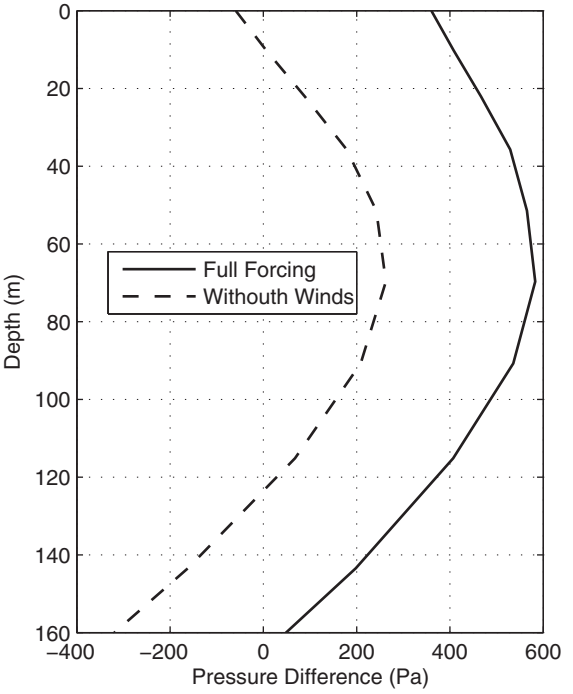


**Figure 15.** Vertical profiles of pressure difference between the Gulf of Aden and the Red Sea averaged from the model results in August 1980.

During August the exchange has a quasi-two-layer structure, with the deep outflow

diminished almost completely (Figure 18). The interface between the upper outflow and lower inflow is located at about 50 m along the strait. The lower layer is composed of cold and low-salinity water with almost uniform properties and is separated by a strong thermocline from the warmer and saltier upper layer.

For both months, the mean along-channel velocities in each layer, hence the layer Froude numbers, vary along the strait, reflecting the changes of the geometric area across the strait (Figures 17 and 18). North of the Perim Narrows, the lateral contraction over the whole depths in the strait increases the mean velocities and the layer Froude numbers in all three layers. Around the Hanish Sill (but not on the sill), the lateral contraction occurs below the surface layer and, therefore, only increases the mean velocities and Froude numbers in the middle layer and bottom layer. The mean velocities on the sill are not locally increased due to a relative wide cross section there.

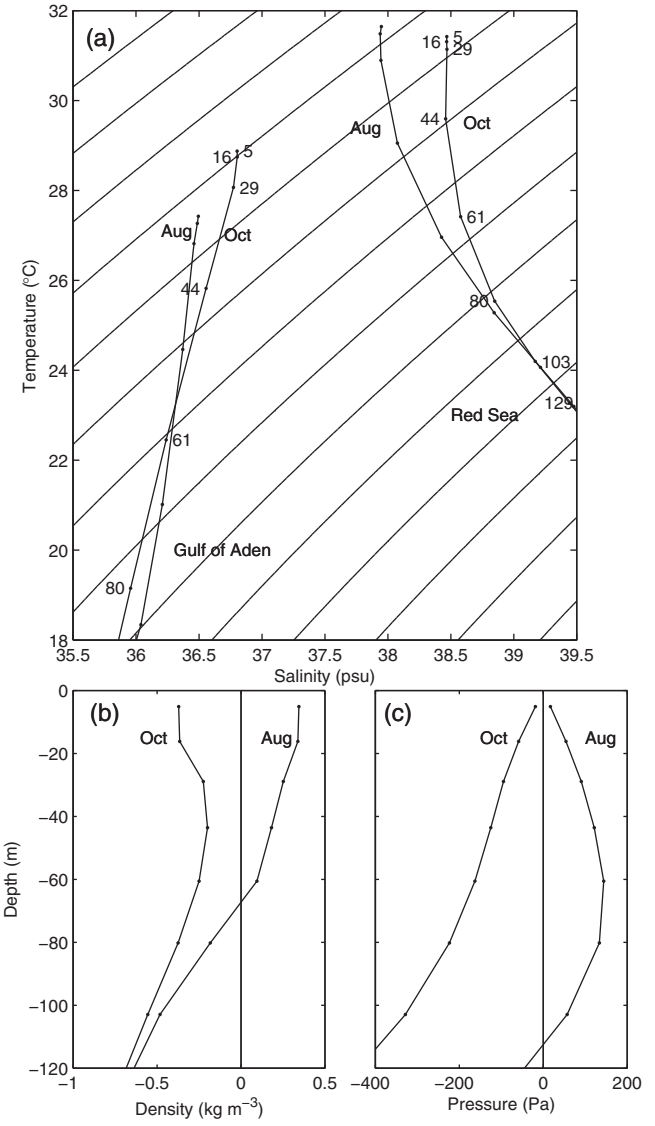


**Figure 16.** Changes of the water properties in the upper layer from August to October. Vertical profiles of temperature and salinity in the Gulf of Aden (averaged around 12°N) and the Red Sea (averaged around 18°N) for August and October are shown in the T-S diagram of Figure 16a, and the numbers denote the depths. The profiles of density difference between the Gulf of Aden and the Red Sea in August and October are shown in Figure 16b. Positive values indicate larger values in the Gulf of Aden. The profiles of pressure difference resulted from the density difference between the Gulf of Aden and the Red Sea are shown in Figure 16c.

In order to examine the criticality of the exchange flows from the layer Froude numbers along the strait, equation (4) can be rearranged as

$$\frac{w_3}{w_2}\tilde{F}_2^2 = -\frac{(\tilde{F}_1^2-1)(\tilde{F}_3^2-1)}{(\tilde{F}_1^2-1)+\beta(\tilde{F}_3^2-1)}, \quad (5)$$

where $\beta = \frac{w_2(1-r)}{w_3 r}$. Equation (5) defines a surface in the space $\left(\tilde{F}_1^2, \frac{w_3}{w_2}\tilde{F}_2^2, \tilde{F}_3^2\right)$ on which the critical conditions for the three-layer exchange flows are satisfied. For a constant value of $\frac{w_3}{w_2}\tilde{F}_2^2$, equation (5) defines curves on the plane of $(\tilde{F}_1^2, \tilde{F}_3^2)$ on which the critical conditions are satisfied, and these critical curves divide the $(\tilde{F}_1^2, \tilde{F}_3^2)$ plane into several regions that correspond to flows being, respectively, subcritical, provisionally supercritical with respect to one wave mode, and provisionally supercritical with respect to both waves modes (see detailed discussion in *Sannino et al.* [2009]. The qualifier "provisionally" is used because the wave speeds may also be imaginary, in which case the hydraulic interpretation is clouded).

Following the method used in *Pickart et al.* [2010], we use the estimated values of $\tilde{F}_1^2$, $\tilde{F}_2^2$, and $\tilde{F}_3^2$ along the strait to assess the hydraulic states of the three-layer exchange flows. For each transect in the strait, the critical curves in the $(\tilde{F}_1^2, \tilde{F}_3^2)$ plane can be plotted

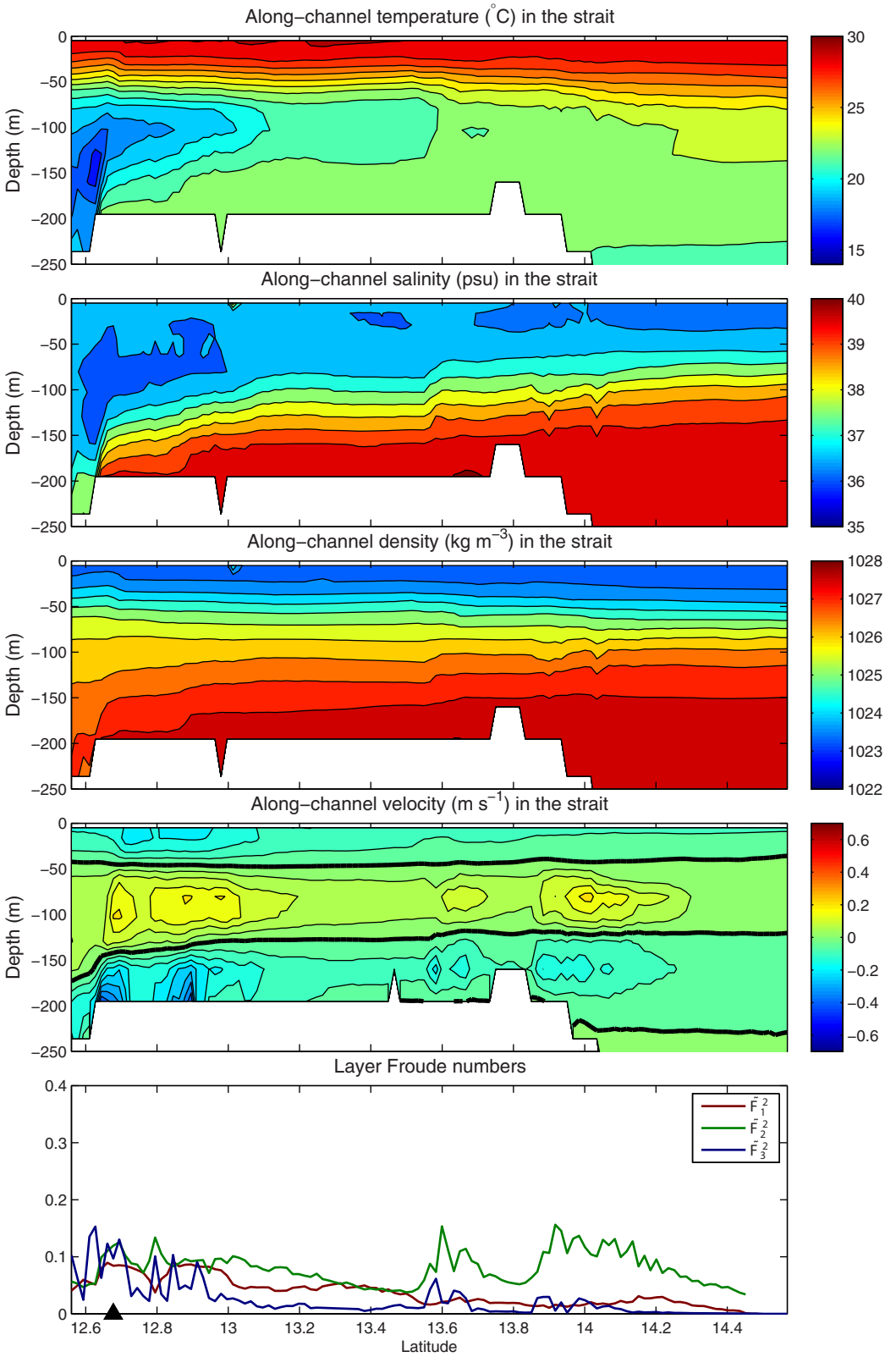


**Figure 17.** Cross-channel averaged salinity, temperature, vertical density, along-channel velocity, and layer Froude number along the strait for June 1980. The black triangle in the bottom panel marks the location of the section in Figure 19.

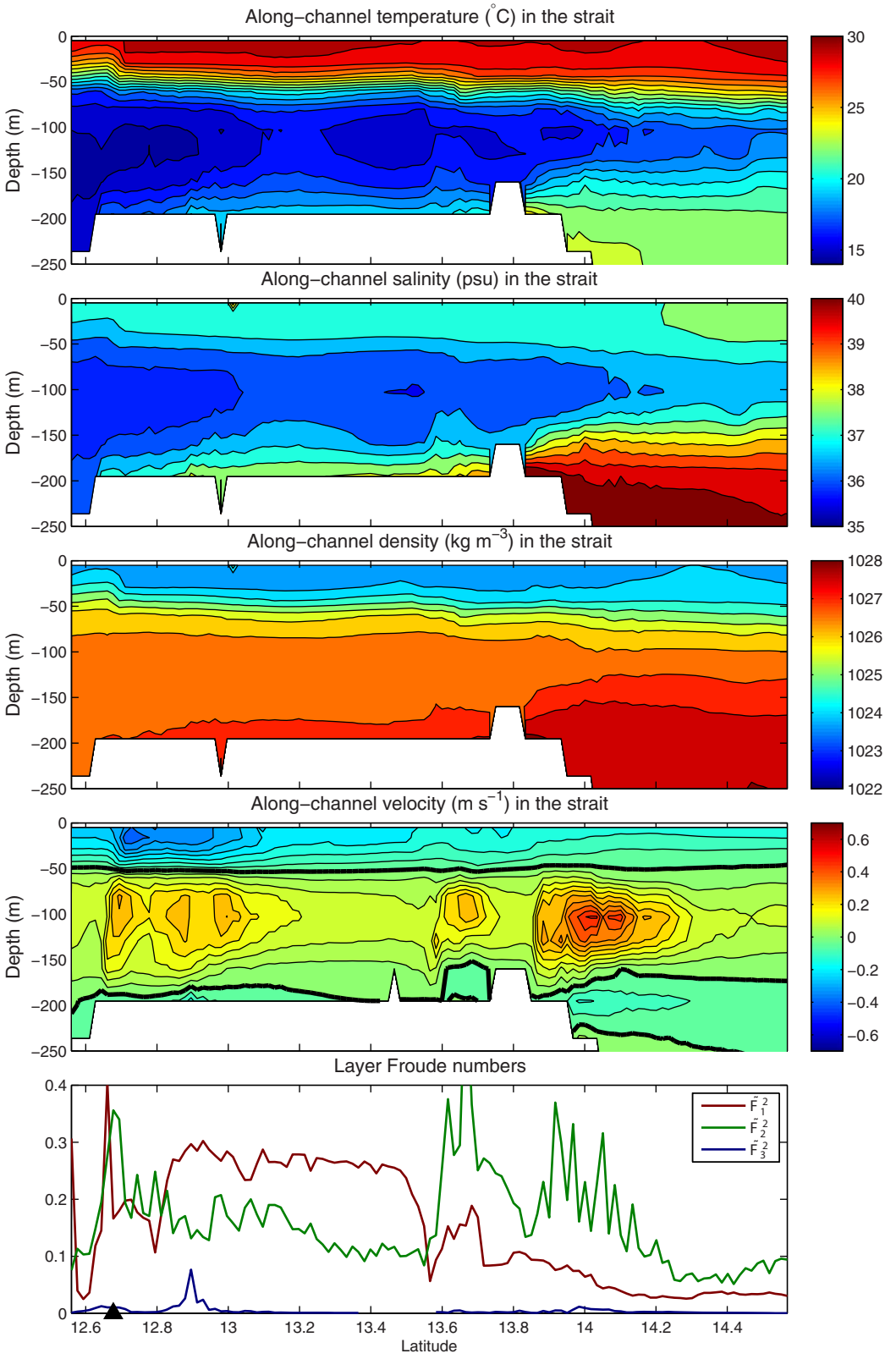


**Figure 18.** Cross-channel averaged salinity, temperature, vertical density, along-channel velocity, and layer Froude number along the strait for August 1980. The black triangle in the bottom panel marks the location of the section in Figure 19.

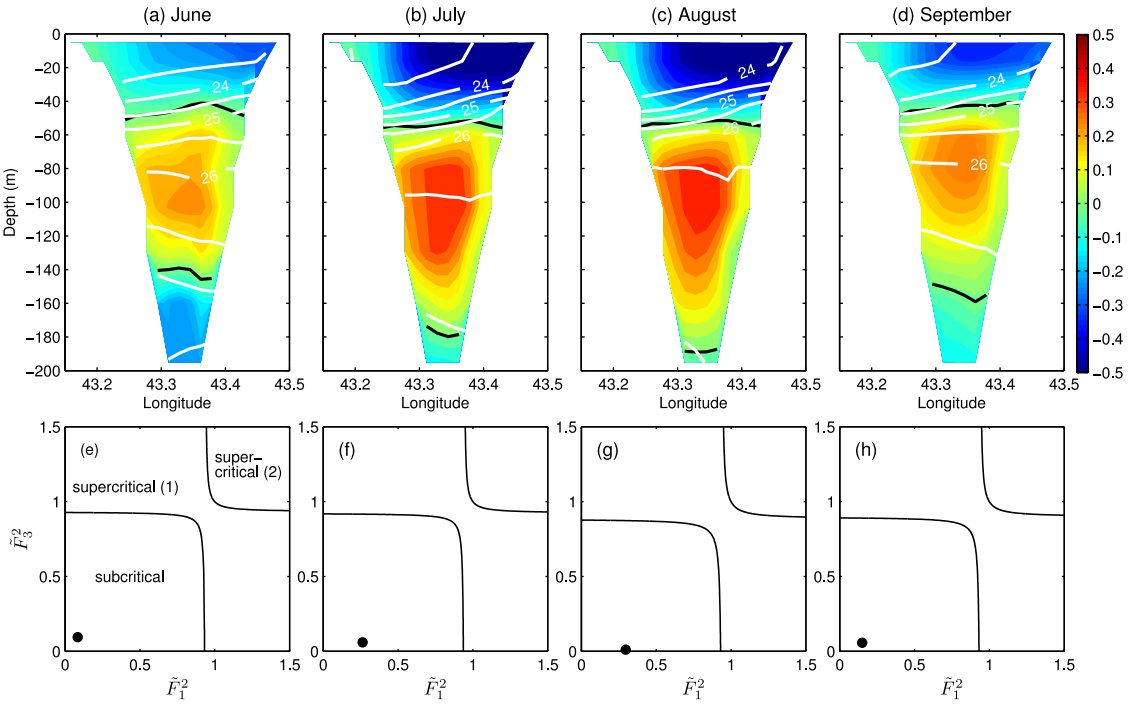


**Figure 19.** Three-layer hydraulics in the strait around the Perim Narrows at the marked location in Figures 17 and 18. (a–d) Cross sections of along-channel velocity (color shading, m $s^{-1}$), potential density anomaly (white contours, kg $m^{-3}$) from June to September 1980. The black lines indicate the zero contours of along-channel velocity. (e–h) Hydraulic states on the $(\tilde{F}_1^2, \tilde{F}_3^2)$ plane for the corresponding sections.

for the estimated $\frac{w_3}{w_2}\tilde{F}_2^2$, then the estimated $(\tilde{F}_1^2, \tilde{F}_3^2)$ can be located on the plane to determine the criticality at the section. Figure 19 shows the results from June to September at one section around the Perim Narrows, where the maximal velocities and Froude numbers in all three layers occur due to the narrowing of channel over the whole depths (Figures 17 and 18). For every summer month, the critical curves determined by the estimated value of $\frac{w_3}{w_2}\tilde{F}_2^2$ at the section divide the $(\tilde{F}_1^2, \tilde{F}_3^2)$ plane into three regions, with the region closest to the origin corresponding to subcritical flow and the farthest corresponding to provisionally supercritical flow with respect to both wave modes. The intermediate region corresponds to flow that is provisionally supercritical with respect to just one wave mode [refer to *Sannino et al.*, 2009] for detailed discussion). In spite of the different vertical structures of the three-layer exchange flows in the strait during the months from June through September, all the hydraulic states represented by the dots lie well within the subcritical region (Figure 19). Results for other sections in the strait, with smaller Froude numbers, lie even closer to origin in the subcritical region. These results suggest that the water exchanges in the strait during the summer overturning circulation are substantially subcritical. This conclusion is consistent with the lack of any prominent hydraulic jump along the strait as shown in Figures 17 and 18 and is also supported by the minor role played by advection in the along-strait momentum balance (Figure 11a).

These findings come with several caveats. One is that the findings of subcriticality apply only to the monthly mean flow. It is possible that hydraulic transitions occur in instantaneous fields over certain time intervals. Second, the model sill depth of 160 m exceeds the value 137 m measured by *Lambeck et al.* [2011]. As a crude estimate of the sensitivity to this discrepancy, we increase velocities at the sill (and decrease the layer thicknesses there), in proportion to the ratio 160/137. The layer Froude numbers at the sill increase, but the sill flow remains subcritical, largely because of the large lateral extent occupied by the upper layer. Finally, the complete lack of hydraulic control seems surprising given that the deep outflow (our layer 3) can be cut off in August. This chocking off of the lowest layer certainly suggests the sort of blocking behavior generally associated with a hydraulic control that is acting preferentially on the lowest layer. One might therefore expect to see some signs of such a control in July, but this is not the case.

## 5. Conclusions

The reversal of the overturning circulation in summer is the most prominent seasonal feature in the Red Sea, and the intrusion of the cold, low-salinity, and nutrient-rich GAIW at intermediate depths is of particular interest because of its potential effect on the biological system in the southern part of the Red Sea [*Triantafyllou et al.*, 2014] (Churchill et al., submitted to, 2013). The objectives of this modeling study are to examine the evolution of GAIW in the Red Sea and to identify the forcing mechanisms that control the amplitude and phase of the intrusion. These results are also important for paleoclimate studies; e.g., *Biton et al*. [2010] suggested a proxy of the intensity of the summer monsoon based on the assumption that the summer monsoonal winds are responsible for the intrusion of GAIW.

The MITgcm simulation successfully reproduces the seasonal exchange pattern in the strait, and the summer intrusion is a robust seasonal feature in the summer overturning circulation in the model. The vertical structure of the summer overturning is revealed for the first time in the model results. The maximum extension of the summer overturning cell in the model reaches almost 24°N, indicative of a much stronger cell than in previous study by *Sofianos and Johns* [2002].

Horizontally, the relatively cold and fresh GAIW in the model forms an eastern boundary current in the southern Red Sea at the depths of 50–100 m. The summer circulation is dominated by anticyclonic eddies in the southern Red Sea. The intrusion of the GAIW is strongly affected by the eddies and is diverted into the interior of the basin from the boundary current during the summer intrusion. The GAIW is trapped in the eddy and gradually mixed with the ambient waters when the overturning circulation is reversed back to the winter type in October and November.

Three forcing mechanisms, including shoaling of the thermocline in the Gulf of Aden, surface wind stress in the Red Sea, and latitudinal heating difference, are identified in the model to be important in controlling the amplitudes and phases of the intrusion. In agreement with the conventional ideas, the model results suggest that the shoaling of the thermocline in the Gulf of Aden is capable of introducing a northward pressure gradient and driving the subsurface intrusion. However, the remote winds in the north Indian Ocean through the ECCO open boundary conditions, instead of local upwelling, are more important in driving the shoaling. This is consistent with the recent modeling study in *Aiki et al*. [2006] and observations in *Bower and Furey* [2012]. Therefore, the open boundary conditions in the Gulf of Aden are critical for successful simulation of the summer overturning circulation.

The surface winds in the Red Sea substantially enhance the overturning circulation and the intrusion of the GAIW as revealed in the model. In the upper layers where the wind stress can penetrate, the surface winds drive the surface outflow directly. A surface slope downward toward the north is established to balance the surface wind stress. At intermediate depths, the surface slope tends to increase the northward baroclinic pressure gradient and the intrusion. Additionally, the latitudinal differential heating by solar insolation in late summer increases the temperature in the upper layer in the Gulf of Aden but decreases the surface temperature in the Red Sea, and the reversed surface currents increase the salinity in the upper layer in the southern Red Sea. These two processes act together to modify the vertical density structure both in the Gulf of Aden and in the Red Sea, therefore, to change the pressure gradient force that drives the subsurface intrusion. These two processes are important to explain the mismatch in the phase between the shoaled thermocline in the Gulf of Aden and the cessation of the intrusion.

The hydraulic states in the strait are rigorously examined using the critical conditions for the three-layer exchange flows. The exchange flows in the strait during the summer months do not appear to be hydraulically controlled. This means that the circulation in the Red Sea is "freely" influenced by the conditions in the Gulf of Aden. At the intermediate depths, the vertical viscosity and lateral friction in the strait act on the intruding flow to balance the northward pressure gradient force.

**Acknowledgments**
Partial support for this effort was provided by the Saudi Aramco Marine Environmental Research Center at KAUST. We thank two reviewers and Hezi Gildor for comments and suggestions that improved the manuscript.

## References

Aiki, H., K. Takahashi, and T. Yamagata (2006), The Red Sea outflow regulated by the Indian monsoon, *Cont. Shelf Res.*, *26*, 1448–1468.
Beal, L. M., A. Ffield, and A. L. Gordon (2000), Spreading of Red Sea overflow waters in the Indian Ocean, *J. Geophys. Res.*, *105*, 8549–8564.
Belkin, I. M. (2009), Rapid warming of Large Marine Ecosystems, *Prog. Oceanogr.*, *81*, 207–213, doi:10.1016/J.Pocean.2009.04.011.
Biton, E., H. Gildor, and W. R. Peltier (2008), Red Sea during the last glacial maximum: Implications for sea level reconstruction, *Paleoceanography*, *23*, PA1214, doi:10.1029/2007PA001431.

Biton, E., H. Gildor, G. Trommer, M. Siccha, M. Kucera, M. T. J. van der Meer, and S. Schouten (2010), Sensitivity of Red Sea circulation to monsoonal variability during the Holocene: An integrated data and modeling study, *Paleoceanography*, *25*, PA4209, doi:10.1029/2009PA001876.

Bower, A. S., and H. H. Furey (2012), Mesoscale eddies in the Gulf of Aden and their impact on the spreading of Red Sea outflow water, *Prog. Oceanogr.*, *96*, 14–39.

Bower, A. S., H. D. Hunt, and J. F. Price (2000), Character and dynamics of the Red Sea and Persian Gulf outflows, *J. Geophys. Res.*, *105*, 6387–6414.

Boyer, T. P., C. Stephens, J. I. Antonov, M. E. Conkright, R. A. Locarnini, T. D. O'Brien, and H. E. Garcia (2002), *World Ocean Atlas 2001, Vol. 2: Salinity*, edited by S. Levitus, NOAA Atlas NESDIS 50, 165 pp., U.S. Gov. Print. Off., Washington, D. C.

Cember, R. P. (1988), On the sources, formation, and circulation of Red-Sea deep-water, *J. Geophys. Res.*, *93*, 8175–8191.

Clifford, M., C. Horton, J. Schmitz, and L. H. Kantha (1997), An oceanographic nowcast/forecast system for the Red Sea, *J. Geophys. Res.*, *102*, 25,101–25,122, doi:10.1029/97JC01919.

Eshel, G., and N. H. Naik (1997), Climatological coastal jet collision, intermediate water formation, and the general circulation of the Red Sea, *J. Phys. Oceanogr.*, *27*, 1233–1257.

Eshel, G., M. A. Cane, and M. B. Blumenthal (1994), Modes of subsurface, intermediate, and deep-water renewal in the Red-Sea, *J. Geophys. Res.*, *99*, 15,941–15,952.

Finnigan, T. D., K. B. Winters, and G. N. Ivey (2001), Response characteristics of a buoyancy-driven sea, *J. Phys. Oceanogr.*, *31*(9), 2721–2736.

Kalnay, E., et al. (1996), The NCEP/NCAR 40-year reanalysis project, *Bull. Am. Meteorol. Soc.*, *77*, 437–471.

Köhl, A., and D. Stammer (2008), Variability of the meridional overturning in the North Atlantic from the 50-year GECCO state estimation, *J. Phys. Oceanogr.*, *38*, 1913–1930.

Lambeck, K., A. Purcell, N. C. Flemming, C. Vita-Finzi, A. M. Alsharekh, and G. N. Bailey (2011), Sea level and shoreline reconstructions for the Red Sea: Isostatic and tectonic considerations and implications for hominin migration out of Africa, *Quat. Sci. Rev.*, *30*(25–26), 3542–3574, doi:10.1016/J.Quascirev.2011.08.008.

Large, W. G., J. C. Mcwilliams, and S. C. Doney (1994), Oceanic vertical mixing—A review and a model with a nonlocal boundary-layer parameterization, *Rev. Geophys.*, *32*, 363–403.

Maillard, C., and G. Soliman (1986), Hydrography of the Red-Sea and exchanges with the Indian-Ocean in summer, *Oceanol. Acta*, *9*, 249–269.

Manasrah, R., M. Badran, H. U. Lass, and W. G. Fennel (2004), Circulation and winter deep-water formation in the northern Red Sea, *Oceanologia*, *46*(1), 5–23.

Marshall, J., C. Hill, L. Perelman, and A. Adcroft (1997), Hydrostatic, quasi-hydrostatic, and nonhydrostatic ocean modeling, *J. Geophys. Res.*, *102*, 5733–5752.

Murray, S. P., and W. Johns (1997), Direct observations of seasonal exchange through the Bab el Mandab Strait, *Geophys. Res. Lett.*, *24*, 2557–2560.

Patzert, W. C. (1974), Wind-induced reversal in Red-Sea circulation, *Deep Sea Res.*, *21*, 109–121.

Phillips, O. M. (1966), On turbulent convection currents and the circulation of the Red Sea, *Deep Sea Res.*, *13*, 1149–1160.

Pickart, R. S., L. J. Pratt, D. J. Torres, T. E. Whitledge, A. Y. Proshutinsky, K. Aagaard, T. A. Agnew, G. W. K. Moore, and H. J. Dail (2010), Evolution and dynamics of the flow through Herald Canyon in the western Chukchi Sea, *Deep Sea Res., Part II*, *57*(1–2), 5–26, doi:10.1016/J.Dsr2.2009.08.002.

Plahn, O., B. Baschek, T. H. Badewien, M. Walter, and M. Rhein (2002), Importance of the Gulf of Aqaba for the formation of bottom water in the Red Sea, *J. Geophys. Res. Oceans*, *107*(C8), 22–1–22-18, doi:10.1029/2000JC000342.

Pratt, L. J. (2008), Critical conditions and composite Froude numbers for layered flow with transverse variations in velocity, *J. Fluid Mech.*, *605*, 281–291.

Pratt, L. J., W. Johns, S. P. Murray, and K. Katsumata (1999), Hydraulic interpretation of direct velocity measurements in the Bab al Mandab, *J. Phys. Oceanogr.*, *29*, 2769–2784.

Pratt, L. J., H. E. Deese, S. P. Murray, and W. Johns (2000), Continuous dynamical modes in straits having arbitrary cross sections, with applications to the Bab al Mandab, *J. Phys. Oceanogr.*, *30*, 2515–2534.

Quadfasel, D., and H. Baudner (1993), Gyre-scale circulation cells in the Red sea, *Oceanol. Acta*, *16*, 221–229.

Raitsos, D. E., I. Hoteit, P. K. Prihartato, T. Chronis, G. Triantafyllou, and Y. Abualnaja (2011), Abrupt warming of the Red Sea, *Geophys. Res. Lett.*, *38*, doi:10.1029/2011gl047984.

Sannino, G., L. Pratt, and A. Carillo (2009), Hydraulic criticality of the exchange flow through the Strait of Gibraltar, *J. Phys. Oceanogr.*, *39*(11), 2779–2799, doi:10.1175/2009jpo4075.1.

Siddall, M., D. A. Smeed, S. Matthiesen, and E. J. Rohling (2002), Modelling the seasonal cycle of the exchange flow in Bab el Mandab (Red Sea), *Deep Sea Res., Part I*, *49*, 1551–1569.

Smeed, D. (1997), Seasonal variation of the flow in the strait of Bah al Mandab, *Oceanol. Acta*, *20*(6), 773–781.

Smeed, D. A. (2000), Hydraulic control of three-layer exchange flows: Application to the Bab al Mandab, *J. Phys. Oceanogr.*, *30*(10), 2574–2588.

Smeed, D. A. (2004), Exchange through the Bab el Mandab, *Deep Sea Res., Part II*, *51*(4-5), 455–474, doi:10.1016/J.Dsr2.2003.11.002.

Sofianos, S., W. E. Johns, and S. P. Murray (2002), Heat and freshwater budgets in the Red Sea from direct observations at Bab el Mandeb, *Deep Sea Res., Part II*, *49*, 1323–1340.

Sofianos, S. S., and W. E. Johns (2001), Wind induced sea level variability in the Red Sea, *Geophys. Res. Lett.*, *28*, 3175–3178.

Sofianos, S. S., and W. E. Johns (2002), An oceanic general circulation model (OGCM) investigation of the Red Sea circulation: 1. Exchange between the Red Sea and the Indian Ocean, *J. Geophys. Res.*, *107*, 3196, doi:10.1029/2001JC001185.

Sofianos, S. S., and W. E. Johns (2003), An oceanic general circulation model (OGCM) investigation of the Red Sea circulation: 2. Three-dimensional circulation in the Red Sea, *J. Geophys. Res.*, *108*(C3), 3066, doi:10.1029/2001JC001185.

Sofianos, S. S., and W. E. Johns (2007), Observations of the summer Red Sea circulation, *J. Geophys. Res.*, *112*, C06025, doi:10.1029/2006JC003886.

Stephens, C., J. I. Antonov, T. P. Boyer, M. E. Conkright, R. A. Locarnini, T. D. O'Brien, and H. E. Garcia (2002), *World Ocean Atlas 2001, Vol. 1: Temperature*, edited by S. Levitus, NOAA Atlas NESDIS 49, 167 pp., U.S. Gov. Print. Off., Washington, D. C.

Tragou, E., and C. Garrett (1997), The shallow thermohaline circulation of the Red Sea, *Deep Sea Res., Part I*, *44*, 1355–1376.

Triantafyllou, G., F. Yao, G. Petihakis, K. P. Tsiaras, D. E. Raitsos, and I. Hoteit (2014), Exploring the Red Sea seasonal ecosystem functioning using a three-dimensional biophysical model, *J. Geophys. Res. Oceans*, *119*, doi:10.1002/2013JC009641.

Woelk, S., and D. Quadfasel (1996), Renewal of deep water in the Red Sea during 1982–1987, *J. Geophys. Res.*, *101*, 18,155–18,165.

Yao, F., I. Hoteit, L. J. Pratt, A. S. Bower, A. Köhl, and D. Rivas (2014), Seasonal overturning circulation in the Red Sea: 2. Winter circulation, *J. Geophys. Res. Oceans*, *119*, doi:10.1002/2013JC009331.